GLIA | WILEY

RESEARCH ARTICLE

Autoimmune neuroinflammation triggers mitochondrial oxidation in oligodendrocytes

Jasmin Steudler[1] | Timothy Ecott[1] | Daniela C. Ivan[1] | Elisa Bouillet[1] |
Sabrina Walthert[1] | Kristina Berve[1] | Tobias P. Dick[2] | Britta Engelhardt[1] |
Giuseppe Locatelli[1] (ID)

[1]Theodor Kocher Institute, University of Bern, Bern, Switzerland

[2]Division of Redox Regulation, DKFZ-ZMBH Alliance, German Cancer Research Center (DKFZ), Heidelberg, Germany

Correspondence
Giuseppe Locatelli, Theodor Kocher Institute, University of Bern, Freiestrasse 1, Postach 938, CH-3012, Bern, Switzerland.
Email: giuseppe.locatelli@novartis.com

Abstract

Oligodendrocytes (ODCs) are myelinating cells of the central nervous system (CNS) supporting neuronal survival. Oxidants and mitochondrial dysfunction have been suggested as the main causes of ODC damage during neuroinflammation as observed in multiple sclerosis (MS). Nonetheless, the dynamics of this process remain unclear, thus hindering the design of neuroprotective therapeutic strategies. To decipher the spatio-temporal pattern of oxidative damage and dysfunction of ODC mitochondria in vivo, we created a novel mouse model in which ODCs selectively express the ratiometric H_2O_2 biosensor mito-roGFP2-Orp1 allowing for quantification of redox changes in their mitochondria. Using 2-photon imaging of the exposed spinal cord, we observed significant mitochondrial oxidation in ODCs upon induction of the MS model experimental autoimmune encephalomyelitis (EAE). This redox change became already apparent during the preclinical phase of EAE prior to CNS infiltration of inflammatory cells. Upon clinical EAE development, mitochondria oxidation remained detectable and was associated with a significant impairment in organelle density and morphology. These alterations correlated with the proximity of ODCs to inflammatory lesions containing activated microglia/macrophages. During the chronic progression of EAE, ODC mitochondria maintained an altered morphology, but their oxidant levels decreased to levels observed in healthy mice. Taken together, our study implicates oxidative stress in ODC mitochondria as a novel pre-clinical sign of MS-like inflammation and demonstrates that evolving redox and morphological changes in mitochondria accompany ODC dysfunction during neuroinflammation.

KEYWORDS
experimental autoimmune encephalomyelitis, mitochondria, multiple sclerosis, myelin, neurodegeneration, oligodendrocyte, reactive species

---

Jasmin Steudler, Timothy Ecott, and Daniela C. Ivan contributed equally to this study.

1 | INTRODUCTION

Multiple sclerosis (MS) is a chronic inflammatory disease of the central nervous system (CNS) characterized by heterogeneous disease presentation, with progressive loss of motor function as common clinical symptom. Histopathologically, the CNS of MS patients displays oligodendrocyte (ODC) death and demyelination, axonal degeneration and multifocal invasion of inflammatory cells. ODCs produce myelin and are metabolically coupled with axons (Fünfschilling et al., 2012; Lee et al., 2012). Accordingly, experimental ODC depletion directly leads to neuronal death (Locatelli et al., 2012) and metabolic impairments in ODCs impact the temporal resolution of axonal firing (Moore et al., 2020). In MS patients, ODCs show altered heterogeneity not only in lesioned sites, but also in the non-inflamed normal-appearing white matter, thus suggesting a widespread dysfunction of these cells in the entire CNS during neuroinflammation (Huynh et al., 2014). Given extensive ODC damage in early CNS lesions devoid of inflammatory infiltrates, some researchers have even proposed that MS may arise from a primary ODC defect, but this hypothesis remains debated (Barnett & Prineas, 2004).

ODCs can suffer from a variety of damaging mechanisms leading to impairment and cell death (Zeis & Schaeren-Wiemers, 2008), together contributing to disease progression in MS and other neurological disorders (Lucchinetti et al., 1999; Zeis & Schaeren-Wiemers, 2008). Among these insults, oxidative stress is a main degenerative process (Haider et al., 2011) caused by the increased presence of reactive oxygen/nitrogen species (ROS/RNS) in the affected CNS tissue. ROS/RNS are tightly regulated signaling mediators (Trachootham et al., 2008) mainly released as by-products of physiological processes. Their intracellular production and detoxification are in a delicate equilibrium that impacts ODC survival in several pathologies (López-Juárez et al., 2017; McIver et al., 2010). Increasing intracellular concentrations of ROS/RNS can lead to DNA damage and lipid peroxidation in ODCs (Haider et al., 2011; Tang et al., 2017). Moreover, ODCs are the largest CNS sink for iron (Todorich et al., 2009), with iron accumulation directly linked to the amplification of ROS/RNS-induced oxidation.

Chiefly responsible for intracellular ROS/RNS production during homeostasis and pathology, mitochondria are dynamic organelles regulating vital physiological processes including energy production, ion homeostasis and anti-apoptotic mechanisms (Knott et al., 2008). ROS/RNS are mainly released by mitochondria because of their metabolic functions (Lacza et al., 2006; Murphy, 2009). At the same time however, mitochondria are highly susceptible to oxidative damage, with metabolic impairment or inflammation causing overproduction of radicals at the level of the oxidative phosphorylation chain and consequent damage to mitochondrial DNA, lipids, and proteins (Mronga et al., 2004; Witte et al., 2014). Oxidative stress in these organelles directly impairs ATP production and diminishes organelle biogenesis, thus creating a vicious circle of self-sustaining cellular dysfunction (Mronga et al., 2004; Rose et al., 2017; Witte et al., 2014). Notably, mitochondrial damage is proposed as a primary factor in ODC pathology during MS, potentially through ROS/RNS mediated mechanisms (Bolaños et al., 1997; Konradi et al., 2012; Lan et al., 2018).

In the complex scenario of CNS inflammation however, ROS/RNS are also massively produced by resident and blood borne myeloid cells. The extracellular release of oxidizing radicals by these immune cells is considered a main agent of tissue destruction in both MS and MS models (Haider et al., 2011; Locatelli et al., 2018; Mendiola et al., 2020). However, the overall role of ROS/RNS remains controversial and context-dependent by driving tissue damage and at the same time decreasing T cell-mediated inflammation in animal models (De Caterina et al., 1995; Niedbala et al., 2011). Taken together, the combined actions of intracellular and immune-mediated ROS/RNS production could drive mitochondrial impairment and dysfunction in ODCs during neuroinflammation. While the therapeutic targeting of oxidative stress would require precise understanding of the spatio-temporal actions of oxidizing radicals, the dynamics of these processes in ODCs during MS and MS-like inflammation remain however speculative.

To visualize the fast spatial and temporal dynamic of oxidation in ODC mitochondria, we created the ODC$^{mitoGFP\text{-}Tomato}$ animal model in which MOG$^+$ mature ODCs express in their mitochondria the ratiometric peroxide sensor mito-roGFP2-Orp1. In this probe, the yeast thiol peroxidase Orp1 is fused to redox-sensitive GFP (roGFP2). Oxidation of Orp1 by peroxides induces the formation of a disulfide bond in roGFP2, altering its fluorescence (Gutscher et al., 2009). Altogether, ratiometric changes in fluorescence emission allow to assess variations in peroxide levels (Fujikawa et al., 2016; Gutscher et al., 2009).

By performing 2-photon imaging of ODC$^{mitoGFP\text{-}Tomato}$ mice induced with the MS model experimental autoimmune encephalomyelitis (EAE), we here observed a significant increase in ODC mitochondria oxidation as soon as 8 days post immunization and until the clinical onset of the disease. Complementary histological analysis showed that at these initial EAE stages, oxidation correlated with higher density and decreased length of ODC mitochondria, both indicative of a disbalanced homeostasis of these organelles and suggesting impaired functionality. Counterintuitively, while mitochondrial length decreased during the subsequent chronic phase of autoimmune neuroinflammation, mitochondrial oxidation returned to homeostatic levels.

Taken together, our data suggest that distinct mechanisms affect mitochondrial physiology in ODCs at the different phases of EAE development. Our experimental platform shows for the first time in vivo that oxidative pathology in ODC mitochondria is an early hallmark of autoimmune neuroinflammation, with dysfunction of these organelles as a key mechanism potentially contributing to ODC pathology.

2 | MATERIAL AND METHODS

2.1 | Animals

iNOS-tdTomato were kindly provided by Prof. Alain Bessis (ENS Paris, France); MOG-cre mice by Prof. Ari Waisman (University of Mainz, Germany); CCR2-RFP x CX3CR1-GFP mice were a gentle gift of Dr. Israel F. Charo (UCSF); mito-roGFP2-Orp1 mice were provided by

Prof. Tobias Dick (University Heidelberg); Ai14 reporter mice are from The Jackson laboratory. Mice were housed in individually ventilated cages under specific pathogen-free conditions. Animal procedures were performed in accordance with the Swiss legislation on the protection of animals and were approved by the veterinary office of the Canton of Bern, Switzerland.

2.2 | Active experimental autoimmune encephalomyelitis induction and control immunization

aEAE was induced in both male and female mice by injection of myelin oligodendrocyte glycoprotein peptide 35–55 (MOG_{35-55} peptide, 200 μg per animal, Genscript) and complete Freund's adjuvant (Incomplete Freund's Adjuvant, Santa Cruz Biotechnology; supplemented with *Mycobacterium tuberculosis*, Difco). An emulsion of MOG_{35-55} and CFA was injected subcutaneously in mouse flanks and at the tail base at day 0; in addition, 300 ng of pertussis toxin (List Biological Laboratories, Campbell, CA) was injected intraperitoneally at day 0 and day 2. As controls served mice treated as above, however with CFA emulsified in Dulbecco's phosphate- buffered saline (DPBS, Gibco, Paisley, UK) without MOG_{35-55}. Immunized mice were weighted and disease development scored daily according to a previously established system (Tietz et al., 2016). Four clinical time points were defined: weight loss (5 animals presenting a 3%–5% loss of weight shortly preceding clinical symptoms), clinical onset (9 animals showing a limb tail and partial hind leg paraparesis, average clinical score ± *SD* 1.03 ± 0.47), symptomatic peak of disease (10 animals presenting hind leg paraparesis and unsteady gait or hind leg paraplegia 4 days after EAE onset, average clinical score ± *SD* 1.6 ± 0.31), chronic EAE (7 animals showing a recovered, yet not complete strength in the hind limbs 10 days after disease onset, average clinical score ± *SD* 0.92 ± 0.31). At day 8 post treatment, 6 mice following CFA + PTx + MOG_{35-55} immunization and 5 mice following CFA +- PTx control immunization were analyzed.

2.3 | Spinal cord isolation and cryostat sections

Mice were sacrificed and transcardially perfused with 4% paraformaldehyde (PFA, Merk Darmstadt, Germany) in DPBS (Gibco, Paisley, UK); isolated spinal cords were post-fixed in 4% PFA overnight, cryopreserved in 30% sucrose (Sigma-Aldrich, St. Louis, MO) diluted in DPBS for 3 days and frozen at −80°C in O.C.T. (Tissue-Tek). 20–25 μm spinal cord longitudinal sections were cut using a cryostat (HM550, Thermo Fisher).

2.4 | Immunofluorescence stainings of CNS tissue

For Iba1, CC1 and NeuN stainings, spinal cord sections were initially fixed with 100% ice cold acetone at −20°C for 10 min and dried before being reconstituted with 1× homemade Tris-buffered saline (1× TBS). For MBP and COX IV staining, sections were fixed with 100% ice cold methanol at −20°C and washed with 1× TBS (3 × 10 min). Unspecific binding was prevented by incubation in 10% goat or donkey serum containing 0.1% Triton (Sigma-Aldrich, St. Louis, MO) diluted in 1× TBS (for Iba1, CC1 and NeuN stainings), 5% BSA containing 0.3% Triton in 1× TBS (for MBP stainings) or 5% FBS in 1× TBS (for COX IV stainings). Following 1× TBS rinsing, the slides were incubated overnight at 4°C with the following primary antibodies: goat anti-Iba1 (NB100-1028, Novus Biologicals, 1:100); mouse anti-CC1 (MABC200, Sigma-Aldrich, 1:200); mouse anti-NeuN (Sigma Millipore Corp, 1:100) (antibodies diluted in 2% goat serum containing 0.1% Triton in TBS), rat anti-MBP (MCA409S, aa82-87, 1:100, diluted in 1% BSA + 0.3% Triton in 1× TBS) and mouse anti-COX IV (Biolegend, Clone 4011-B3,E8, Cat. 937,802, 1:100, diluted in 1× FBS). After tissue rinsing 3 × 10 min with 1× TBS, the slices were incubated for 2 h at RT in the following secondary antibodies: Alexa Fluor 647 goat anti-mouse IgG (Invitrogen, stock 2 mg/mL), donkey anti-goat AF647 IgG (H + L) (Jackson ImmunoResearch) (diluted at 1:200 in 2% goat serum in 1× TBS for CC1, NeuN and Iba1 stainings or in 1× FBS in 1× TBS for the COX IV staining), goat anti-rat AF647 (diluted at 1:200 in 1% BSA in 1× TBS). Following 1× TBS wash (3x10 min), the sections were incubated with DAPI (1:5000 in 1× TBS, 1 mg/ml stock, AppliChem, Darmstadt, Germany) for 10 min at RT and mounted with Mowiol 4-88 (Sigma-Aldrich, St Louis, MO).

Analysis of MBP immunostaining was performed on images acquired with a 20× objective of a fluorescence microscope (Nikon, Eclipse E600). For the other stainings, Z-stack images of CNS sections were acquired using a LSM800 confocal microscope (Zeiss) with 40x magnification and analyzed using Fiji (National Institute of Health, Bethesda, MD). The shape factor of single ODC mitochondria was assessed by hand-drawing the length and width of single organelle puncta via Fiji and calculating their ratio via Excel. Distinct puncta were identified by manually reducing the intensity of fluorescence in the GFP channel before the analysis, to confirm the physical separation of individual signals. The density of ODC mitochondria was assessed manually by defining the tdTomato$^+$ cytosolic cell body surrounding the nucleus and by counting the number of identifiable mitochondria puncta within the area. Iba1$^+$-containing lesions were defined as cluster accumulations of at least 4 DAPI$^+$ Iba1$^+$ myeloid cells disrupting the normal-appearing tissue organization. The categories "close," "intermediate," and "far" in relationship to distance from such lesions were assigned as a measure of proximity to cellular sources of ROS/RNS.

2.5 | Flow cytometry

CX3CR1-GFP x CCR2-RFP mice were sacrificed at indicated time points following induction of EAE; non-immunized littermates were used as healthy controls. Following perfusion with 1× PBS, brain and spinal cord tissues were isolated and placed in ice cold 1× PBS. Each organ was cut into small pieces and digested at 37°C for 30 min in HBSS$^{Mg + Cl+}$ containing 0.4 mg/ml collagenase VIII and 1 μg/ml DNase (Roche). Tissue homogenization was performed in glass homogenizers using dissection media (3 ml/organ) containing

HBSS$^{Mg + Cl+}$, 25 mM HEPES buffer solution (Gibco, Paisley, UK) and 45% glucose dissolved in sterile water. Following filtration through 70 μm strainers (SPL Life Sciences, Cat. 93,070) and washing with FACS buffer (PBS + 2% Fetal Calf Serum–SeraGlob), cell gradient was performed using 37% Percoll (Ge Healthcare Biosciences, Cat. 17-0891-01) and centrifugation at 800 g, for 30 min at 4°C. This step allowed the creation of a density gradient formed by a myelin ring at the surface, a middle layer containing CNS resident and infiltrating myeloid cells and a blood cell ring at the bottom of the tube. The middle layer was filtered through 70 μm cell strainer and washed. Following centrifugation (10 min, 1200 rpm, 4°C), the supernatant was discarded, and the cells were prepared for antibody staining. Cells were incubated with blocking anti-CD16/32 (homemade) for 15 min on ice. After washing, cells were incubated for 30 min at 4°C, in dark conditions, with the following antibodies diluted in FACS buffer: CD3 (AF700 anti-mouse, clone 17A2, Biolegend, Cat. 100216), CD11b (PercP anti-mouse/human, clone M1/70, Biolegend, Cat. 101230), CD45 (PE/Cy7 anti-mouse, clone 30F11, Biolegend 103114) and Ly6G (APC anti-mouse, Clone 1A8, Biolegend, Cat. 127614). Detection of ROS production was performed via deep red CellROX staining (Thermo Fisher) according to the manufacturer instructions. Cells isolated from inguinal lymph nodes of C57BL6/j mice (Charles River laboratories) were used for compensations and instrument set-up. The samples were acquired using an Attune NxT cytometer (Thermo Fisher Scientific). A total volume of 250 μl was analyzed per sample. Analysis was performed using the FlowJoTM software (version 10, Ashland). Following the identification of populations of interest based on size and granularity, we performed the downstream analysis on single cell populations and identified infiltrating monocytes as CD45^{high}CD11b$^+$ CCR2$^+$CX3CR1^{neg}, granulocytes as CD45^{high}CD11b$^+$ CCR2^{neg} Ly6G$^+$, lymphocytes as CD45^{high}CD11b^{neg}CD3$^+$ and microglia as CD45^{intermediate}CD11b$^+$ CX3CR1$^+$CCR2^{neg}.

2.6 | Two-photon intravital microscopy

The cervical spinal cord was exposed by laminectomy as previously described (Haghayegh Jahromi et al., 2017). Briefly, animals were intubated by insertion of a canula in the trachea providing oxygen and isoflurane through a Minivent system (Harvard apparatus). Laminectomy (C2-5) was performed and spinal column fixed at C1 and C6 in a stereotactic frame. Body temperature and heart rate were recorded and stored electronically. To provide treatment access, dura mater was carefully removed prior to imaging using a needle and forceps (Romanelli et al., 2013), and tissue superfused with a warm homemade CSF solution (Locatelli et al., 2018). Incubation with reagents was performed on the exposed spinal cord for a minimum of 10′ in warm CSF (DTT, Sigma Aldrich; H_2O_2, Merck; Fluoromyelin red staining, Invitrogen). Imaging was performed via 2-photon (LaVision Trim-Scope II microscope, Spectra-Physics laser). Mouse respiration via MiniVent was synchronized to picture acquisition through a triggering device (TrigViFo) reducing imaging artifacts (Vladymyrov et al., 2020). Through an additional toolkit (VivoFollow II) (Vladymyrov et al., 2020),

this synchronization allowed real-time distortion correction. Tissue displacement was automatically corrected by objective and stage adjustment through a Python script (VivoFollow I) (Vladymyrov et al., 2016). Single images, z-stacks, and videos were acquired with ImSpector software (LaVision). For ratiometric mito-roGFP2-Orp1 imaging, 3D volumes of the spinal cord were acquired twice, alternating 800 and 940 nm wavelengths (3% laser power, 1041 × 1041 pixel resolution, 800 Hz speed; for representative images: 940 nm, 3.8% laser power, 2041 × 2041 resolution, 600 Hz speed, PMT gain 60%, step-size 1 μm). Raw images were processed with Fiji (Schindelin et al., 2012) and saved as TIF. Region of interests were created around cells/structures/mitochondria and fluorescence analyzed after background subtraction. Distinct mitochondria puncta were identified by manually reducing the intensity of fluorescence in the GFP channel in Fiji before the analysis, to confirm the physical separation of individual mitochondria.

2.7 | Statistics

Statistical analysis was performed using GraphPad Prism 9 software (La Jolla, CA). All values are presented as box and whiskers (min to max). Datasets were first tested for normality using the Shapiro–Wilk normality test. Kruskal-Wallis test with Dunn's multiple comparison test was then used to compare 3 or more experimental groups and Mann Whitney U test was used to compare 2 groups. For the flow cytometry analysis and animal-based comparisons in Figures 2b,h and 3b,e,g,i,n, one-way ANOVA with post hoc Bonferroni's comparison was performed. Asterisks indicate significant differences (*p < .05, **p < .01 and ***p < .001, ****p < .0001).

3 | RESULTS

3.1 | Validation of the ODC$^{mitoGFP-Tomato}$ animal model

To study and visualize ODC mitochondrial pathology in a mouse model, we crossed MOG-cre mice (Hövelmeyer et al.) to cre-inducible mito-roGFP2-Orp1 mice (Fujikawa et al., 2016) and cre-inducible tdTomato reporter (Ai14) mice (Madisen et al., 2010). In the resulting MOG-cre x mito-roGFP2-Orp1 x Ai14 model (henceforth ODC$^{mitoGFP-Tomato}$; Figure 1a), GFP$^+$ mitochondria could be detected in the tdTomato$^+$ ODC cell body and cytoplasmic extensions, together allowing to visualize the distribution of these organelles in the complex ODC cytoarchitecture (Figure 1b and Supplementary Movie). To exclude potential MOG-cre-driven recombination in neuronal cells (Frühbeis et al., 2013), we stained CNS sections of ODC$^{mitoGFP-Tomato}$ mice for the ODC marker CC1 and for the neuronal marker NeuN and found that 95% of roGFP2$^+$ tdTomato$^+$ cells stained positive for CC1 (Figure 1c).

Next, we analyzed expression and detection range of the mito-roGFP2-Orp1 sensor in vivo. We exposed the cervical spinal cord of ODC$^{mitoGFP-Tomato}$ mice by laminectomy and observed that ODC-specific tdTomato and mito-ORP1-roGFP2 expression could be
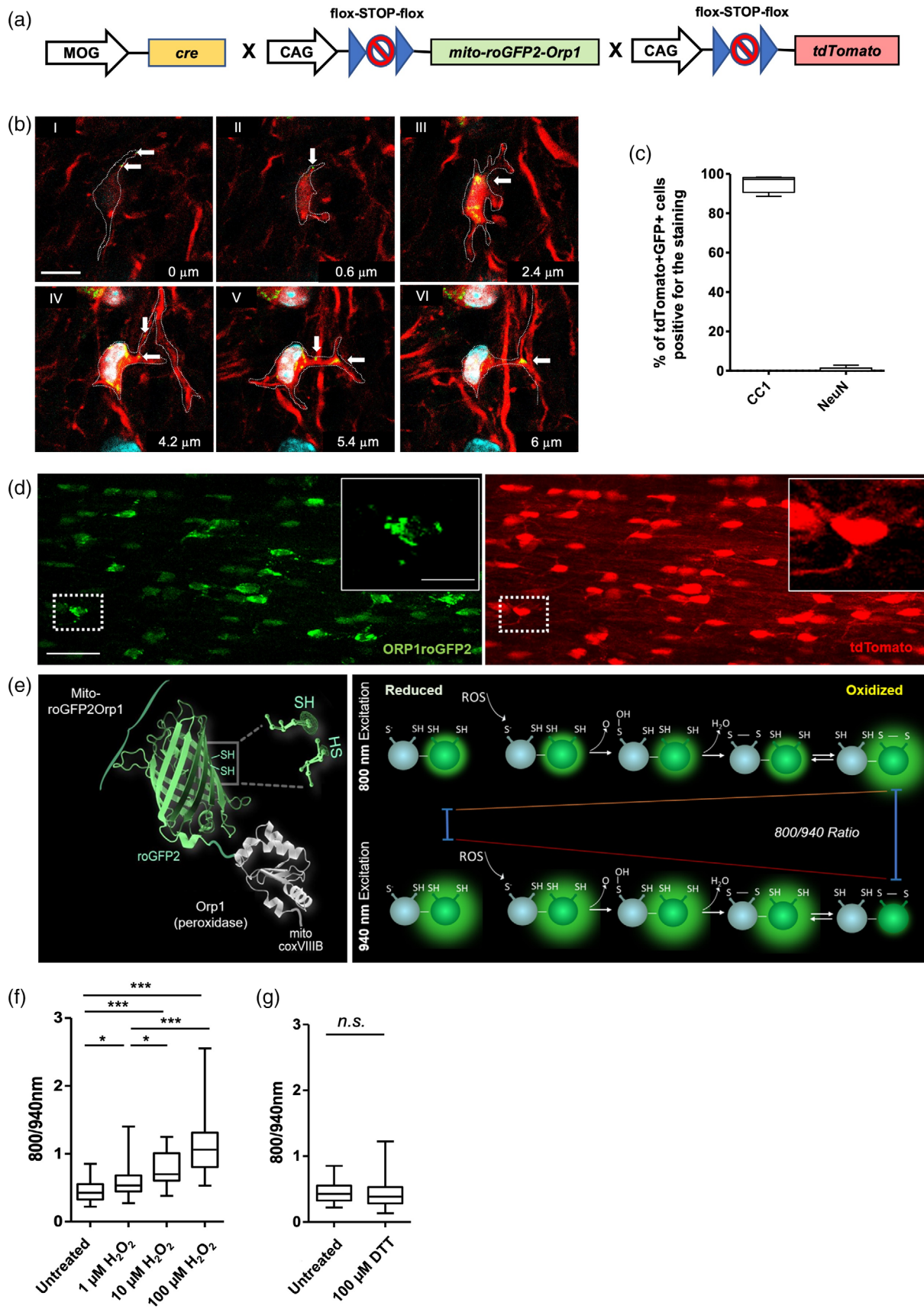
FIGURE 1 Legend on next page.

reliably detected in the spinal cord white matter (Figure 1d). We assessed the detection range of the mitochondrial sensor in ODCs by incubating the exposed spinal cord of healthy ODC[mitoGFP-Tomato] mice with increasing amounts of hydrogen peroxide (1–10 to 100 μM). In our system, upon 2-photon excitation at 800 and 940 nm, the ratio of mito-roGFP2-Orp1 emission intensities is directly related to the degree of probe oxidation (Meyer & Dick, 2010) (Figure 1e). Moreover, given its ratiometric characteristics, mito-roGFP2-Orp1 senses peroxide without being perturbed by photobleaching or variations in expression (Gutscher et al., 2009). Sensor oxidation significantly increased over the untreated baseline values after incubation with 1 μM peroxide and reached the expected maximum detection range (circa 2.5 fold increase over basal conditions) following incubation with 100 μM peroxide, as reported in previous studies (Breckwoldt et al., 2014) (Figure 1f). Incubation with dithiothreitol (DTT; 100 μM), a disulfide reductant, did not lead to a significant decrease in probe oxidation, thus suggesting an overall reduced basal state of ODC mitochondria during homeostasis (Figure 1g).

In summary, ODC[mitoGFP-Tomato] mice allowed to detect a wide range of peroxide concentrations in ODC mitochondria in vivo. This mouse model can thus be used to assess changes in the redox state of ODC mitochondria in a pathological context.

3.2 | ODC mitochondria are oxidized upon development of autoimmune neuroinflammation

ROS/RNS have been proposed as main drivers of tissue damage in MS (Smith, 2011), but their subcellular distribution and temporal dissemination during neuroinflammation remain unclear. To shed light on oxidative mechanisms specifically in ODC mitochondria, we assessed mito-roGFP2-Orp1 emission intensity in vivo in ODC[mitoGFP-Tomato] mice during the course of EAE. Notably, we observed a significant increase in mitochondrial oxidation at the first clinical signs of EAE development, that is, when animals started losing weight 10–11 days after immunization ("weight loss"), and upon the subsequent onset of motor symptoms (Figures 2a,b and S1a). At these early stages, mito-roGFP2-Orp1 emission in ODC mitochondria resembled values

detected after exposing healthy spinal cords to 1–10 μM of peroxide (Figure 2c). This higher oxidative state observed at the time when mice started to lose weight could be significantly decreased in vivo by spinal cord incubation with DTT, thus showing that, in principle, ODC mitochondrial oxidation could be pharmacologically reversed during EAE (Figure 2d).

Subsequent analysis of ODC mitochondrial oxidation at the symptomatic peak of EAE (4 days after clinical onset, Figure S1b) showed a strong heterogeneity in ODC oxidation, with a minority of ODCs containing highly oxidized mitochondria (Figure 2a,e) and a vast majority of ODCs showing a significant decrease in roGFP2-Orp1 oxidation reaching values observed in non-immunized control mice (Figure 2a,b). Surprisingly, analysis of ODC[mitoGFP-Tomato] mice at the chronic stage of the disease (10 days after onset of clinical symptoms, Figure S1c) revealed that mitochondria oxidation in ODCs further decreased becoming comparable to untreated mice (Figure 2b) and to the DTT-induced fully reduced state detected in healthy spinal cords (Figure 2f).

To assess whether mitochondria oxidation correlated with myelin loss, we immunostained spinal cord tissue sections from ODC[mitoGFP-Tomato] mice with an anti-MBP antibody. A significant decrease in MBP staining could be observed at all analyzed timepoints of clinical disease, with the strongest loss at disease onset (Figure S1d,e). Thus, no direct correlation between ODC oxidation and demyelination could be observed at the tissue level.

Taken together, in vivo imaging of the spinal cord of ODC[mitoGFP-Tomato] mice during EAE revealed a complex evolution of the mitochondrial redox state in ODCs, with an increase in oxidation at the preclinical and clinical stages of disease development and a subsequent decrease along the chronic phases of EAE. These data highlight how pathological processes affecting the physiology of ODC mitochondria are already dominant at the very beginning of CNS inflammation.

3.3 | Pre-clinical mitochondrial oxidation is detected in absence of CNS-invading immune cells

Earlier work in murine EAE models has shown that mitochondria malfunctioning in CNS cells can occur several days before the first clinical

FIGURE 1 Expression and detection range of the Mito-roGFP2-Orp1 sensor in ODC[mitoGFP-Tomato] mice. (a) Diagram illustrating the genetic make-up of ODC[mitoGFP-Tomato] mice. (b) Representative mitochondrial distribution in a roGFP2[+]tdTomato[+] ODC from a 4%PFA-fixed spinal cord tissue of a ODC[mitoGFP-Tomato] mouse. In green, mitochondrial signal; in red, cytosolic signal, in cyan, nuclei (DAPI). Shown are selected planes (with indicated depth in μm) from the imaged z-stack, illustrating detection of single mitochondria (white arrows) in the main cytosolic processes and in non-compact myelin (quadrant V–VI). Scale bar, 10 μm. (c) Spinal cord from ODC[mitoGFP-Tomato] mice were isolated and 20 μm thick sections stained with anti-APC clone CC1 (left) and NeuN (right). Shown is the percentage of colocalization of roGFP[+] tdTomato^{+} cells with CC1 and NeuN, $n = 5$. (d) In vivo maximum intensity projection of the spinal cord of a ODC[mitoGFP-Tomato] mouse. Green signal (roGFP2) identifies ODC mitochondria, red signal (tdTomato) ODC cytosol, 2-photon wavelength used was 940 nm, laser power 3.5%, 1024×1024 pixel. Scale bar, 20 μm; magnified inlet, scale bar, 8 μm. (e) Structure of the Mito-roGFP2-Orp1 protein, showing cysteine residues reactive to oxidation. roGFP2-Orp1 possesses a mitochondrial-targeting sequence (coxVIIIB) allowing import to the organelle matrix. Depending on the 2-photon excitation wavelength used (right), oxidation increases (at 800 nm) or decreases fluorescence (940 nm). Oxidation sensed by ORP1 is transferred with fast kinetics to roGFP2. (f,g) 800/940 nm emission ratio recorded via 2-photon imaging of the spinal cord of ODC[mitoGFP-Tomato] mice. Shown are box and whiskers graphs with number of mitochondria averaged per single ODC. Peroxide (f) and DTT (g) were incubated for 10′ on the exposed tissue at the indicated concentrations, 5 mice per group, untreated cells, $n = 42$, 1 μM peroxide, $n = 43$, 10 μM peroxide, $n = 38$, 100 μM peroxide, $n = 45$, DTT, $n = 49$. Kruskal-Wallis test with Dunn's multiple comparison test, *$p < .05$; ***$p < .0001$ (f) and Mann Whitney U test (g).
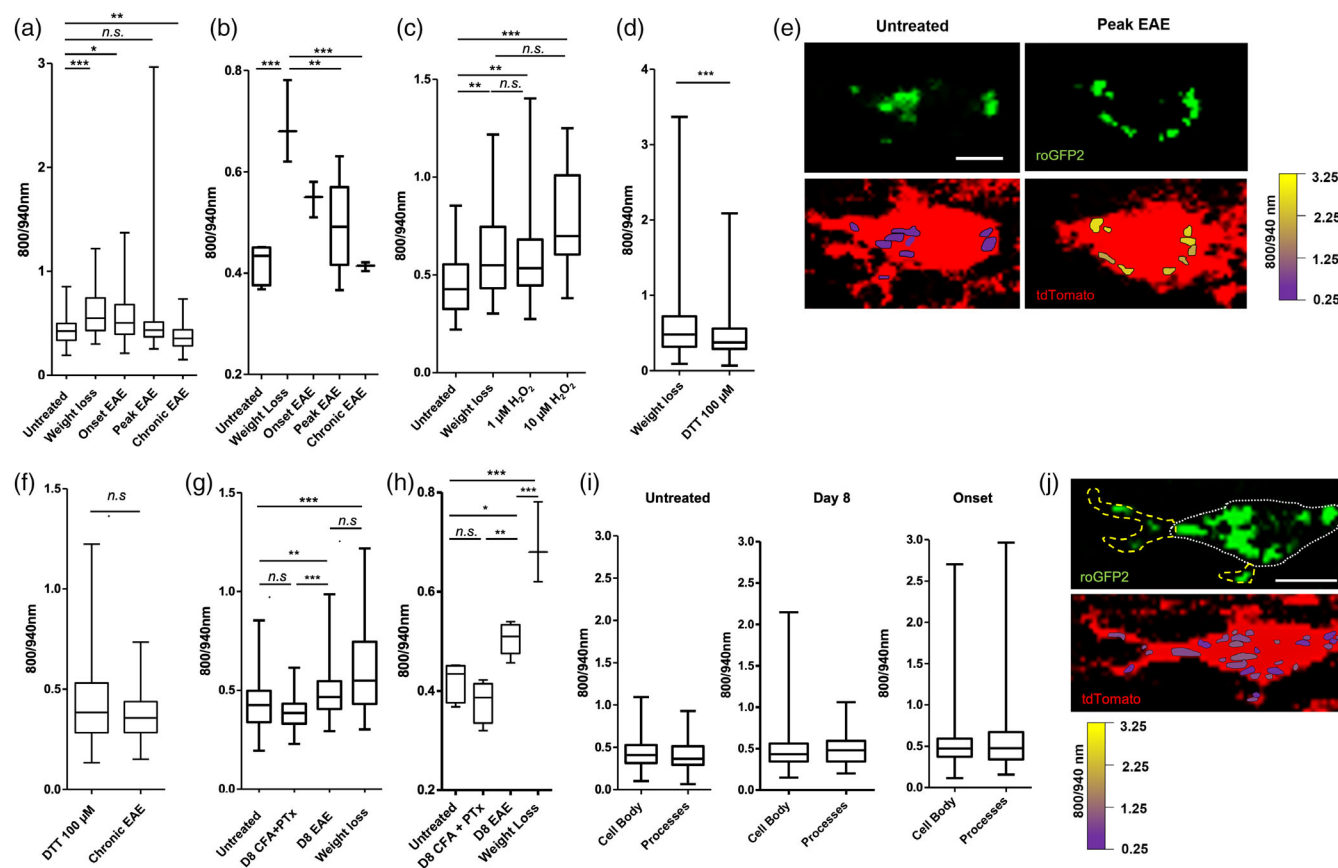
FIGURE 2 In vivo imaging in ODC$^{mitoGFP-Tomato}$ mice shows mitochondrial oxidation in ODCs upon induction of anti-myelin immunity. (a) 800/940 nm 2-photon emission ratio of the spinal cord of ODC$^{mitoGFP-Tomato}$ mice at steady state and at the indicated stages of EAE development. Shown are box and whiskers representations with number of mitochondria averaged per single ODC. Cells from untreated, $n = 650$ ($n = 6$ mice); weight loss, $n = 353$ ($n = 3$ mice); onset, $n = 692$ ($n = 3$ mice); peak $n = 1067$ ($n = 5$ mice); chronic EAE, $n = 450$ ($n = 3$ mice). (b) Box and whiskers representations of single mice from (a). (c) 800/940 nm ratio of the spinal cord of ODC$^{mitoGFP-Tomato}$ mice in untreated mice ($n = 6$), at the weight loss stage of EAE ($n = 3$) or following incubation with peroxide as in Figure 1f ($n = 5$). (d) 800/940 nm ratio of the spinal cord of ODC$^{mitoGFP-Tomato}$ mice at the weight loss stage of EAE before treatment (left, $n = 336$) and following incubation with DTT (right, $n = 226$) (n. of mice per group $= 3$). Shown are values from single mitochondria. (e) Representative 2-photon images of ODCs in the cervical spinal cord of ODC$^{mitoGFP-Tomato}$ mice. Green signal (roGFP2) identifies ODC mitochondria, red signal (tdTomato) cytosol. False color scale indicates 800/940 nm values of single mitochondria puncta. Scale bar, 4 μm. (f) 800/940 nm ratio recorded via 2-photon imaging of spinal cords of healthy ODC$^{mitoGFP-Tomato}$ mice following incubation with DTT ($n = 5$) or in EAE mice at the during chronic EAE ($n = 3$). (g) 800/940 nm emission ratio of the spinal cord of ODC$^{mitoGFP-Tomato}$ mice at steady state and at the indicated stages of EAE development; D8, day 8 post MOG$_{35-55}$ immunization; D8 CFA + PTx, day 8 post injection of CFA and PTx; box and whiskers representations with number of mitochondria averaged per single ODC or h) per single mouse. Cells from untreated, $n = 650$ ($n = 6$ mice); weight loss, $n = 353$ ($n = 3$ mice); D8, $n = 133$ ($n = 5$ mice); D8 CFA + PTx $n = 132$ ($n = 4$ mice). (i) 800/940 nm emission ratio of the spinal cord of ODC$^{mitoGFP-Tomato}$ mice at steady state and at the indicated stages of EAE development. Datapoints correspond to averaged values of mitochondria puncta from the same ODC. Number of mice analyzed: Untreated, $n = 3$; day 8 post immunization, $n = 5$; onset, $n = 5$. (j) Representative 2-photon images of ODCs in the cervical spinal cord of ODC$^{mitoGFP-Tomato}$ mice at day 8 post MOG + CFA immunization. Green signal (roGFP2) identifies ODC mitochondria, red signal (tdTomato) cytosol. False color scale indicates 800/940 nm values of single mitochondria puncta. White dotted line indicates mitochondria assigned to the "cell body," yellow dashed line indicates mitochondria assigned to "processes." Scale bar, 4 μm. (a,c,g) Kruskal-Wallis test with Dunn's multiple comparison test, $*p < .05$; $**p < .001$; $***p < .0001$. (b,h) 1-way ANOVA with Bonferroni's post hoc comparison, $*p < .05$; $**p < .001$; $***p < .0001$. (d,f,i) Mann Whitney U test, $***p < .0001$

signs of disease, thus suggesting that the initial dysfunction might be initially independent from the infiltration of peripheral inflammatory players (Hasseldam et al., 2016; Qi et al., 2006). To test this hypothesis in our model, we investigated ODC oxidation 8 days post immunization, a timepoint in which peripherally activated immune cells have not yet invaded the CNS. To confirm the latter, we induced EAE in a reporter mouse model, CCR2-RFP x CX3CR1-GFP (Saederup et al., 2010),

allowing to distinguish tissue-invading RFP$^+$ inflammatory monocytes from RFP^{negative} GFP$^+$ resident microglia/macrophages. In vivo imaging of these mice at day 8 post immunization revealed that invading RFP$^+$ cells were absent from the exposed cervical spinal cord (data not shown). To extend our analysis to the entire CNS, we performed flow cytometry analysis of isolated brain and spinal cord tissue 8 days post immunization. We observed that microglia numbers were unchanged

compared to non-immunized control mice and no invading lympho-cytes, monocytes or granulocytes were detectable in the spinal cord (Figure S2a) and brain (data not shown) of immunized mice.

Furthermore, the enzyme producing NO, iNOS, was not expressed in CNS cells (data not shown) and ROS production could not be detected in microglia cells at this timepoint (Figure S2b).
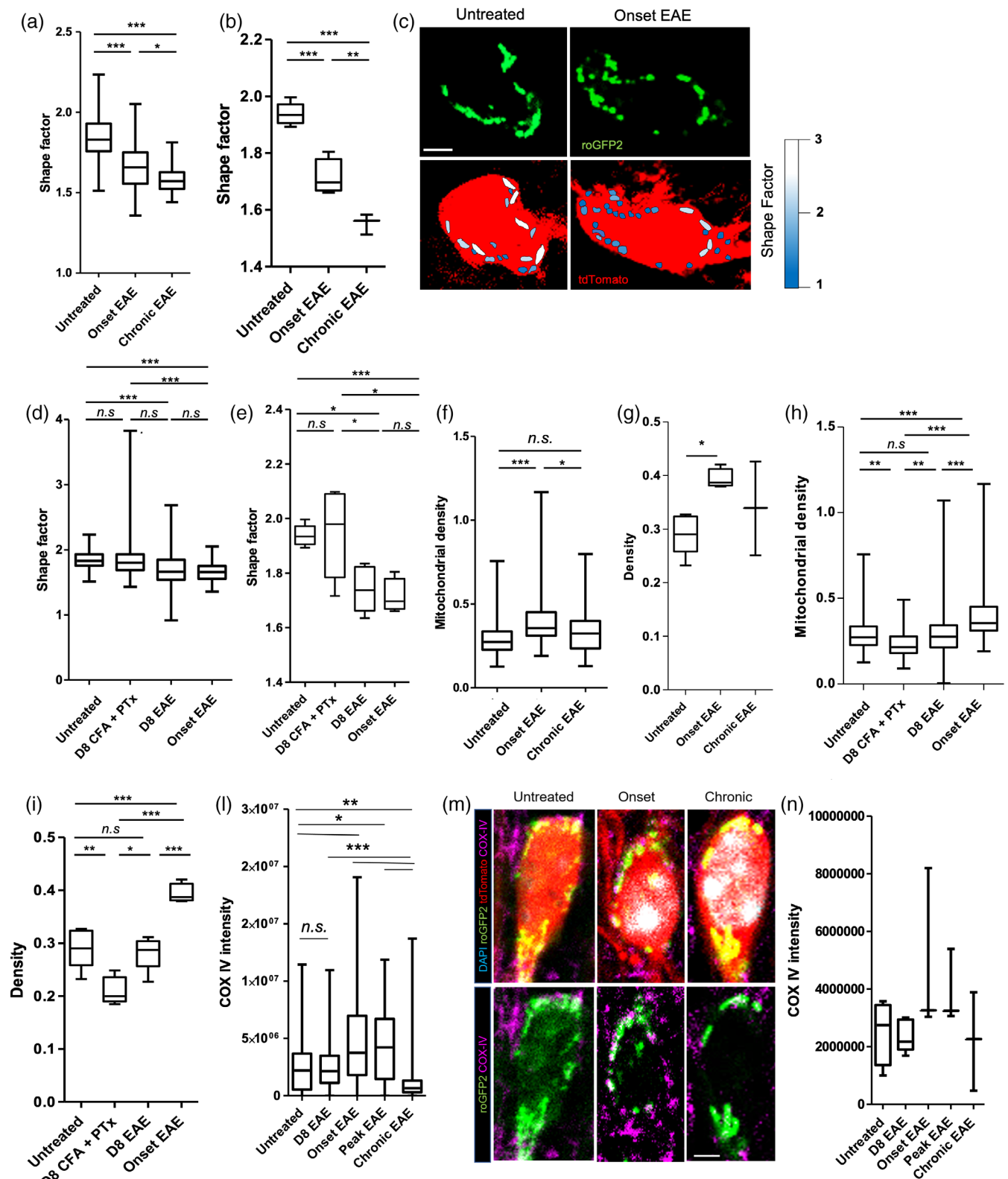

FIGURE 3 Legend on next page.

Notably however, analysis of mito-roGFP2-Orp1 emission in the spinal cord of ODC^mitoGFP-Tomato mice indicated that ODC mitochondria were significantly oxidized at this early stage (Figure 2g,h).

As the adjuvants used during EAE induction can activate the innate immune system also in absence of a CNS-specific autoimmune response (Billiau & Matthys, 2001; Hofstetter et al., 2002), we assessed whether the observed redox changes in ODC mitochondria were caused by the administration of complete Freund's adjuvant (CFA) and pertussis toxin (PTx) in mice. We thus injected ODC^mitoGFP-Tomato mice with CFA and PTx (without MOG_{35-55}) and analyzed mito-roGFP2-Orp1 emission by 2-photon imaging. Treatment with CFA and PTx alone did not affect ODC mitochondrial oxidation (Figure 2g,h), strongly indicating that the observed redox changes in ODCs required the full development of anti-CNS immunity.

In this context, previous work suggested that during autoimmune CNS pathology ODC dysfunction progresses in a "dying-back" fashion with myelin sheaths and distal processes degenerating despite the survival of the ODC cell body (Romanelli et al., 2016). To understand whether oxidation could affect ODC mitochondria in distal cytosolic processes prior to the mitochondria in the ODC cell body, we separately analyzed the redox state of mitochondria located in direct vicinity to the nucleus versus in cytoplasmic extensions at the preclinical and early clinical stages of EAE. At both timepoints, we observed comparable oxidative states in mitochondria close to the nucleus and in distal processes, thus demonstrating that mitochondrial oxidation within the ODC does not depend on the subcellular localization (Figure 2i,j). However, it remains unclear whether a homogeneous degree of oxidative damage would have similar functional consequences in differentially located ODC mitochondria.

Taken together, preclinical analysis of ODC^mitoGFP-Tomato mice showed that a significant increase in ODC mitochondria oxidation precedes the infiltration of peripheral immune cell in the CNS. At the same time, the observed redox changes were dependent on the mounting of anti-myelin immune responses that follows immunization of mice against MOG_{35-55}.

3.4 | Impaired mitochondrial density, morphology, and complex IV expression in ODCs during the course of EAE

The morphology of a mitochondrion is highly dynamic and regulated by different mechanisms including fusion and fission, in turn maintaining physiological mitochondrial distribution and density (Knott et al., 2008). Changes in mitochondria morphology directly correlate with the well-being of these organelles (Garcia et al., 2019), with a reduced shape factor (length/width of the single mitochondria) indicative of decreased functionality and ATP production. However, how neuroinflammation affects the shape of mitochondria in ODCs remains undetermined.

To assess the latter in our model, we analyzed the shape factor of ODC mitochondria in spinal cord sections of healthy and EAE-affected ODC^mitoGFP-Tomato mice by confocal microscopy. Upon onset of clinical EAE, we observed a significant decrease in the ODC mitochondria shape factor compared to ODCs from healthy animals (Figure 3a–c). The shape factor further decreased in ODCs at the chronic stage of disease (Figure 3a,b). To assess whether this change of morphology could already be detected at the preclinical stages, we analyzed tissue from ODC^mitoGFP-Tomato mice 8 days post immunization and found that the shape factor of ODC mitochondria was already significantly lower compared to healthy mice and not different from mice at clinical onset (Figure 3d,e). Conversely, administration of CFA + PTx (without MOG_{35-55}) in ODC^mitoGFP-Tomato mice did not cause detectable morphological changes in ODC mitochondria, again indicating that mitochondrial impairment is not caused by adjuvant-induced immune cell activation but rather by specific development of an anti-CNS immune response (Figure 3d,e).

To understand whether mitochondrial numbers were also affected during EAE, we analyzed ODC mitochondria density in spinal cord sections from ODC^mitoGFP-Tomato mice. Compared to ODCs in healthy animals, mice at clinical onset of EAE displayed a significantly higher mitochondria density within ODCs, while mice at the chronic stage of the disease displayed ODC organelle density similar to control mice (Figure 3f,g). Analysis of tissue from ODC^mitoGFP-Tomato mice

FIGURE 3 Histological analysis of ODC mitochondria shows impairment in organelle morphology and density upon EAE induction. (a–n) ODC^mitoGFP-Tomato mice were perfused, spinal cord tissue isolated and 4% PFA-fixed 20 μm thick sections were analyzed by confocal microscopy. (a) Shown is shape factor (length/width of single puncta) of mitochondria averaged per single ODC or (b) per single mouse. Untreated, no. of cells = 145 (n = 5 mice); onset, n = 80 (n = 4 mice); chronic EAE n = 60 (n = 3 mice). (c) Representative images of ODCs analyzed as in (a). Green signal (roGFP2) identifies ODC mitochondria, red signal (tdTomato) cytosolic ODC structures. False color scale indicates shape factor of single mitochondria puncta. Scale bar, 3 μm. (d) Box and whiskers representations with the shape factor (length/width of single puncta) of mitochondria averaged per single ODC or (e) single mouse. Untreated, no. of cells = 145 (n = 5 mice); day 8 post injection of CFA and PTx, n = 70 (n = 4 mice); day 8 post immunization, n = 120 (n = 5 mice); onset, n = 80 (n = 4 mice). (f–i) Density of mitochondria averaged per single ODC cell body (f,h) or per mouse (g,i). Untreated, n = 145 (n = 5 mice); onset, n = 80 (n = 4 mice); day 8 post injection of CFA and PTx, n = 70 (n = 4 mice); day 8 post immunization, n = 120 (n = 5 mice); chronic EAE n = 60 (n = 3 mice). (l) Box and whiskers representations of background-subtracted COX-IV immunostaining intensity detected in GFP^+ mitochondria, averaged per single ODC. Untreated, no. of cells = 65 (n = 4 mice); D8, n = 88 (n = 5 mice); onset, n = 55 (n = 3 mice); symptomatic peak, n = 50 (n = 3 mice); chronic EAE n = 50 (n = 3 mice). (m) Representative images of ODCs analyzed as in (l). Green signal (roGFP2) identifies ODC mitochondria, red signal (tdTomato) cytosolic ODC structures, magenta COX-IV immunostaining. Scale bar, 3 μm. (n) Box and whiskers representations of mice from (l). (a,d,f,h,l) Kruskal-Wallis test with Dunn's multiple comparison test, (b,e,g,i,n) 1-way ANOVA with Bonferroni post-hoc comparison, *p < .05; **p < .001; ***p < .0001
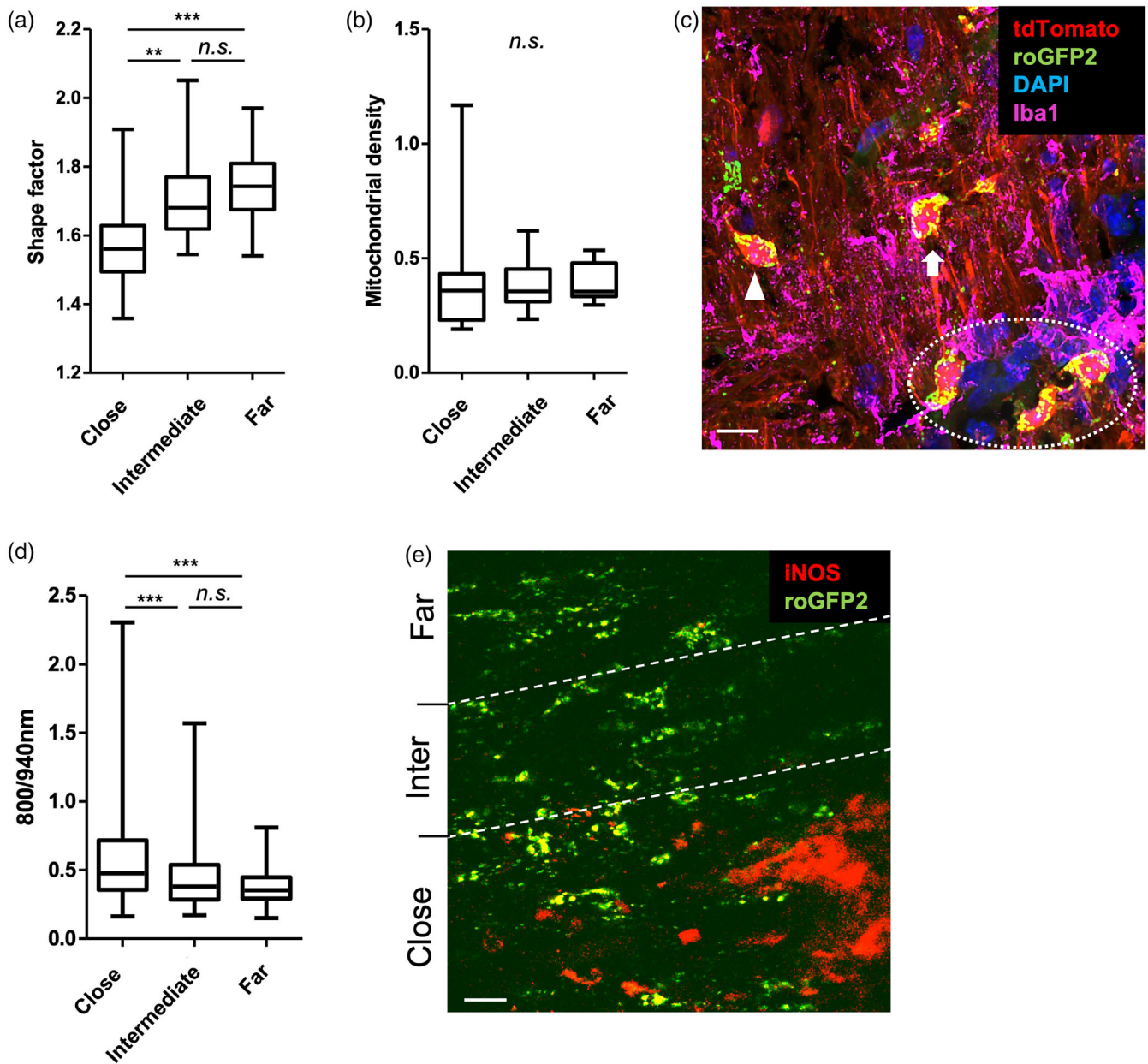
FIGURE 4 Proximity of ODC mitochondria to activated microglia/macrophages correlates with dysfunction. (a–c) ODC$^{mitoGFP-Tomato}$ mice were perfused at onset EAE, spinal cord tissue isolated and PFA-fixed 20 μm thick sections stained with an anti-Iba1 antibody and analyzed by confocal microscopy, $n = 4$. (a,b) Box and whiskers representation with the (a) shape factor (length/width of single puncta) and (b) the density of mitochondria averaged per single ODC. Cells within 20 μm from Iba1$^+$ lesions (close), $n = 30$; cells between 20 μm and 40 μm from Iba1$^+$ lesions (intermediate), $n = 25$; cells further than 40 μm from Iba1$^+$ lesions (far) $n = 25$. (c) Representative images of ODCs from ODC$^{mitoGFP-Tomato}$ mice analyzed as in (a). Green signal (roGFP2) identifies ODC mitochondria, red signal (tdTomato) cytosolic ODC structures, blue signal indicates nuclei (DAPI), magenta indicates Iba1$^+$ cells. Arrow-head indicates a "far" ODC, white arrow a "intermediate" ODC, encircled "close" ODCs. Scale bar, 8 μm. (d,e) ODC$^{mitoGFP-iNOS}$ mice were analyzed by 2-photon imaging of the cervical spinal cord at the onset of EAE, $n = 3$. (d) 800/940 nm emission ratio of Mito-ORP1-roGFP2; shown are mitochondria averaged per single ODC. Cells within 20 μm from iNOS$^+$ cells (close), $n = 50$; cells between 20 and 40 μm from iNOS$^+$ cells (intermediate), $n = 20$; cells further than 40 μm from iNOS$^+$ cells (far) $n = 30$. (e) Representative 2-photon image of ODCs in the cervical spinal cord of ODC$^{mitoGFP-iNOS}$ mice. Green signal (roGFP2) identifies ODC mitochondria, red signal iNOS$^+$ cells. Scale bar, 13 μm. (a,b,d) Kruskal-Wallis test with Dunn's multiple comparison test, *$p < .05$; **$p < .001$; ***$p < .0001$

isolated at preclinical EAE (day 8 p.i.) showed that ODC mitochondrial density was not affected at this stage, while control treatment with CFA + PTx resulted in a significant decrease of organelle density in the ODC cell body compared to both healthy tissue and tissue from EAE-induced mice at day 8 p.i. (Figure 3h,i).

Finally, to indirectly assess whether neuroinflammation impacted oxidative phosphorylation in ODC mitochondria, we immunostained spinal cord sections of untreated and EAE-induced ODC$^{mitoGFP-Tomato}$ mice with an antibody detecting the complex IV subunit COX-IV. Complex IV/cytochrome c oxidase is a key enzymatic complex

pumping protons across the mitochondrial membrane and consuming oxygen for ATP production (Mahad et al., 2008). Compared to ODCs from untreated mice, the intensity of COX-IV expression in ODC mitochondria generally increased at clinical onset and EAE symptomatic peak but decreased during the chronic stage of disease (Figure 3l,m). However, these changes were not significant when comparing single mice (Figure 3n).

In summary, induction of EAE in ODC^{mitoGFP-Tomato} mice led to an impairment in ODC mitochondrial morphology that became apparent at preclinical stages and reached its maximum during the chronic stages of the pathology. At the same time, the density of ODC mitochondria increased significantly at the clinical onset of EAE but decreased to homeostatic levels at the chronic stages of EAE. Together, our analysis suggests that autoimmune CNS inflammation induces not only oxidative stress but also substantial and progressive changes in mitochondria homeostasis and function in ODCs.

3.5 | Microglia/macrophage actions increase ODC mitochondrial dysfunction during EAE

During neuroinflammation, myeloid cells are proposed as main agents of oxidative damage induced to ODCs through their release of ROS/RNS (Mishra & Yong, 2016; Murray & Wynn, 2011). These radicals have different half-lives which directly affect their extracellular distribution in the CNS, with peroxide potentially able to diffuse up to 100 μm in distance from its cellular source (Ledo et al., 2022; Santos et al., 2010).

To understand the contribution of activated myeloid cells to ODC mitochondrial dysfunction during EAE, we first assessed whether ODC mitochondria morphological changes were influenced by the proximity to microglia/macrophage-containing inflammatory lesions. Spinal cord tissue sections from ODC^{mitoGFP-Tomato} mice sacrificed at EAE onset were stained with an anti-Iba1 antibody, revealing the presence of both microglia and CNS-infiltrating monocyte-derived cells. At this stage of EAE, Iba1⁺ lesions inevitably contain ROS/RNS-producing microglia/macrophages (Locatelli et al., 2018; Mendiola et al., 2020) (Figure S2b). We analyzed mitochondria shape factor and density in ODCs adjacent to inflammatory accumulations of Iba1⁺ cells ("close," at less than 20 μm distance from the outermost Iba1⁺ cells – presumably exposed to a higher ROS/RNS concentration), in ODCs situated within an intermediate distance range (20–40 μm distance from lesions - defined as "intermediate"), as well as in ODCs far from the lesion site (>40 μm from Iba1⁺ cellular accumulations - defined as "far"). Mitochondrial shape factor was significantly lower in ODCs situated close to accumulation of Iba1⁺ cells, compared to ODCs located further away from inflammatory lesions (Figure 4a,c). Density of these organelles was however unaffected by proximity to lesions (Figure 4b).

Secondly, we assessed whether the redox state of ODC mitochondria would be similarly influenced by proximity to activated microglia/macrophages. As the mito-roGFP2-Orp1 sensor may suffer artefactual oxidation in fixed tissues, unless properly conserved with alkylating agents (Fujikawa et al., 2016), we again made use of intravital 2-photon imaging. To visualize ROS/RNS-releasing myeloid cells in vivo, we crossed MOG-cre x mito-roGFP2-Orp1 mice to iNOS-tdTomato reporter mice (Béchade et al., 2014), hence obtaining the ODC^{mitoGFP-iNOS} model. Our previous work showed that iNOS⁺ cells in the spinal cord of EAE-induced mice act as key tissue damaging players secreting ROS/RNS starting from the weight loss phase of disease (Locatelli et al., 2018). Accordingly, analysis of ODC^{mitoGFP-iNOS} mice at EAE onset showed that ODC proximity to iNOS⁺ myeloid cells correlated with an increase in mitochondrial redox state, with ODCs within 20 μm of distance from iNOS⁺ cells showing significantly more oxidation compared to farther cells (Figure 4d,e).

In summary, upon clinical development of autoimmune CNS inflammation, both morphology and oxidative stress of ODC mitochondria appear significantly affected by the proximity of myeloid cell-containing inflammatory lesions. Thus, at these stages of EAE, direct actions of activated microglia/macrophages substantially contributed to the progressive dysfunction of ODC mitochondria.

4 | DISCUSSION

ODC dysfunction is a pathological trait common to several CNS conditions (McTigue & Tripathi, 2008). In MS lesions, ODCs are thought to survive the initial demyelinating attack (Wolswijk, 2000) while suffering a "centripetal" damage with myelin degeneration spreading progressively through distal processes toward the cell body (Romanelli et al., 2016). At the same time, analysis of ODC density in the CNS of MS patients demonstrates that ODC cell death is highly heterogeneous, with certain lesions showing complete loss of ODCs and others showing numbers of ODCs exceeding those found in the periplaque white matter (Zeis & Schaeren-Wimers, 2008). These distinct patterns of cellular degeneration appear patient-specific and conserved over time (Metz et al., 2014). Overall, this high variability in ODC damage suggests that dysfunction in these cells during anti-myelin immunity is likely context-dependent and potentially caused by non-overlapping mechanisms.

In this context, ample evidence indicates oxidative stress and mitochondrial pathology as main agents of ODC degeneration (Witte et al., 2014). Diffuse ODC positivity for malondialdehyde and oxidized phospholipids in CNS tissue from MS patients directly implicates oxidative damage as an important contributor to demyelination (Haider et al., 2011). Abundant iron storages and physiologically low levels of antioxidants in ODCs can amplify oxidative stress-induced dysfunction specifically in this cell type (Lassmann & van Horssen, 2016). Accordingly, homeostatic control of oxidation is an essential requisite for cell survival, as demonstrated by the higher susceptibility of mice to cuprizone intoxication following an ODC-specific deletion of the antioxidant regulator Nrf2 (Nellessen et al., 2020). Oxidative stress in ODCs is strongly interlinked to mitochondrial damage (Roth & Núñez, 2016), with inflammation decreasing ODC mitochondrial function (Minchenberg & Massa, 2019). In turn, mitochondrial stress and energetic impairment in ODCs can potentially affect the metabolically

connected axons (Fünfschilling et al., 2012; Y. Lee et al., 2012) and further contribute to worsening of clinical symptoms in MS patients. Mitochondria are extremely sensitive to damage induced by ROS/RNS (Higgins et al., 2010) and possess detoxifying mechanisms including manganese superoxide dismutase and catalase (Ibrahim et al., 2000). Pharmacological support of these anti-oxidative processes significantly protects ODCs upon lysolecithin-induced demyelination (Chamberlain et al., 2017). In certain MS lesions, ODCs were found to lack the COX-I and COX-IV mitochondrial subunit, an alteration potentially caused by NO and indicative of impaired oxidative phosphorylation (Mahad et al., 2008). Analysis of mitochondrial DNA also showed the presence of mutations specific to MS patients in genes encoding for functional proteins including COX-I (Al-Kafaji et al., 2022; Poursadegh Zonouzi et al., 2014).

Despite this considerable body of evidence, the spatial and temporal dynamics of mitochondrial pathology and oxidative dysfunction in ODCs during neuroinflammation remain unclear. We thus created a transgenic mouse model to directly visualize oxidative status and morphology of ODC mitochondria in vivo and in real time through expression of roGFP2-Orp1 (Gutscher et al., 2009). Recent work highlighted the potential of roGFP2-based imaging to assess the mechanisms leading to, for example, transection-induced axonal degeneration (Breckwoldt et al., 2014), and oxidative stress in a Parkinson's disease model (Sanchez-Padilla et al., 2014).

In our study, 2-photon imaging revealed significant ODC mitochondrial oxidation upon induction of anti-myelin inflammation in the spinal cord of ODC$^{mitoGFP-Tomato}$ mice. The observed redox changes were not caused by adjuvants and were thus not triggered by general activation of immune cells but specifically related to the development of anti-myelin immunity. Mitochondrial oxidation could be reversed by treatment with a reducing agent and was comparable to changes induced by tissue exposure to 1–10 μM peroxide. However, while the roGFP2-Orp1 probe reports mainly on the presence of hydrogen peroxide, it can also respond to peroxynitrite and hypochlorite (Müller et al., 2017). Hence, our study does not allow to assess exactly which oxidants caused the observed changes. Notably, a substantial increase in oxidation was detected as early as 8 days after MOG$_{35-55}$ immunization, a timepoint in which peripheral leukocytes did not yet invade the CNS and ROS/RNS production could not be detected in CNS cells. At these initial stages of EAE, ODC mitochondria also displayed a significantly decreased shape factor, a morphological change highly suggestive of impaired functionality (Breckwoldt et al., 2014; Nikić et al., 2011).

Our observations at preclinical stages of EAE are in accordance with earlier work in murine models showing that mitochondrial oxidative dysfunction in CNS cell types precede the formation of inflammatory lesions (Hasseldam et al., 2016; Qi et al., 2006). The mechanism behind this pre-clinical increase in ODC mitochondrial oxidation remains undefined but we hypothesize two partially overlapping causes: (I) thanks to their anatomical proximity to blood vessels, microglia and astrocytes sense the formation of peripheral anti-CNS immunity (Ivan et al., 2021; Sanmarco et al., 2021; Simpson & Oliver, 2020) and release inflammatory molecules directly or indirectly

leading to oxidation of ODC mitochondria; (II) ODC metabolism becomes affected by toxic molecules or subtle alterations in blood supply which follow EAE induction (Rosko et al., 2019) together leading to organelle malfunction and intrinsic overproduction of reactive species at the level of the oxidative phosphorylation complexes. Connecting these two scenarios, earlier work showed that ODCs suffering from mitochondrial stress release inflammatory cytokines and chemokines (Scheld et al., 2019) and thus potentially support the activation of surrounding glial cells triggering a deleterious loop propagating oxidative dysfunction at preclinical stages (Murphy, 2009).

At the subsequent beginning of clinical EAE however, peripheral leukocytes including ROS/RNS-producing monocyte-derived cells massively infiltrate the CNS leading to tissue damage (Locatelli et al., 2018). Activated myeloid cells secrete ROS through NADPH oxidase complexes, myeloperoxidases, and xanthine oxidases (Bedard & Krause, 2007). RNS production is instead regulated by the metabolism of L-arginine, which is catabolized to NO and L-citrulline by the enzyme iNOS (Locatelli et al., 2018; Rath et al., 2014). Beside mediating tissue damage, iNOS-produced NO shows an anti-inflammatory role by decreasing endothelial and Th17 cell activation, thus highlighting its context-dependent effects during neuroinflammation (De Caterina et al., 1995; Niedbala et al., 2011). During EAE, ROS/RNS can be produced by both activated CNS-resident microglia (Simpson & Oliver, 2020) and blood borne monocyte-derived macrophages (Locatelli et al., 2018), which respectively proliferate and invade the CNS and together contribute to the formation of myeloid-cell dominated CNS lesions (Jordão et al., 2019; Saederup et al., 2010). Despite the ability of some ROS to diffuse extracellularly to a relatively long distance from their cellular source (Ledo et al., 2022), the high reactivity of radicals will presumably affect cells near ROS/RNS production to a higher degree. At clinical disease onset in ODC$^{mitoGFP-Tomato}$ mice, ODC mitochondria accordingly displayed: (I) compromised morphology in close proximity to lesions containing Iba1$^+$ microglia/macrophages, and (II) higher oxidation state close to iNOS$^+$ microglia/macrophages. Myeloid cells are known effectors of myelin damage in EAE (Romanelli et al., 2016; Yamasaki et al., 2014), and iNOS-produced NO can directly block oxidative phosphorylation and cause mitochondria dysfunction (Mahad et al., 2015; Tengan & Moraes, 2017).

Taken together, our data suggest that oxidative impairment in ODC mitochondria is a novel and reliable early marker of anti-myelin adaptive immunity. Furthermore, our work indicates that during preclinical and clinical neuroinflammation, mitochondria dysfunction is likely triggered by distinct stage-dependent cellular mechanisms.

During the progression of EAE toward the chronic stages, oxidation in ODC mitochondria however decreased appearing comparable to the homeostatic levels detected in healthy animals. It is tempting to correlate this reduction in oxidative stress to the anti-inflammatory evolution of immune cell players in the inflamed CNS following clinical onset. In particular, we described the progressive functional changes in CNS-invading monocyte-derived cells, switching from ROS/RNS-producing iNOS$^+$ to a dominant tissue-repair Arginase-1$^+$ phenotype along disease progression (Locatelli et al., 2018). Nonetheless, ODCs

at the chronic stages of EAE showed an impaired mitochondrial morphology and lower expression of the complex IV subunit COX-IV compared to both clinical onset and steady-state. Thus, even in absence of diffuse oxidation, ODC mitochondria remain chronically affected also at later stages of disease.

The evolution of mitochondrial morphology is typically regulated by the fusion and fission processes that govern organelle homeostasis (Tondera et al., 2009). While fission leads to the elimination of dysfunctional mitochondria (Twig et al., 2008), organelle fusion is considered a defense mechanism that reduces impairment through the exchange of damaged DNA between organelles (Tondera et al., 2009). Accordingly, alteration in the equilibrium between these mechanisms, especially following radical-induced mitochondria fragmentation (Wu et al., 2011), results in bioenergetic dysfunction and cell damage (Hoppins et al., 2007) potentially leading to cell death (Lee et al., 2021). Accordingly in both MS tissue and in the EAE model, early pathology in spinal cord axons is characterized by a reduced mitochondrial shape factor suggesting loss of function in these organelles (Nikić et al., 2011). In our work, decreased shape factor and increased density of ODC mitochondria at EAE onset suggest a ROS/RNS-induced fragmentation potentially circumventing fusion mechanisms. During the chronic stages of EAE however, ODC mitochondria display a strongly decreased shape factor but density and redox state comparable to mitochondria in healthy animals. Whether these morphological changes at chronic EAE are a long-term consequence of the preceding oxidative stress or caused by temporally distinct mechanisms remains to be addressed. Nonetheless, the normal density and oxidation of mitochondria at this stage would suggest a recovery of homeostatic fusion-fission and anti-oxidant mechanisms in ODCs following the initial phases of clinical neuroinflammation.

Our study has several limitations. First, whether the described changes in ODC mitochondria directly influence myelin stability and clinical presentation in the EAE model remains unaddressed. Mitochondria oxidation was only observed pre-clinically and at the clinical onset of EAE but not in later disease phases, however demyelination and clinical symptoms were clearly detectable in ODC$^{mitoGFP-Tomato}$ mice until the chronic phase of disease. Thus, oxidative stress in ODC mitochondria seems to generally precede tissue damage and disease presentation. Nonetheless, only a correlative analysis of myelin stability at the single cell level would reveal whether mitochondrial impairment is a direct driver of demyelination. While we could visualize compact myelin in vivo via incubation of the spinal cord with a Fluoromyelin dye (Romanelli et al., 2013) (data not shown), the dense distribution of reporter signal in ODC$^{mitoGFP-Tomato}$ mice and the intrinsic limitations of 2-photon resolution did not allow to connect the status of myelinated sheaths to ODC mitochondria at a single cell level. Other approaches, for instance in vivo sparse labeling of ODCs via rabies virus infection (Romanelli et al., 2016), might shed light on the potential causality between mitochondrial dysfunction and demyelination.

Secondly, despite changes in COX-IV immunoreactivity would suggest variations in ATP production at the different stages of EAE (Mahad et al., 2008), our work did not functionally assess whether neuroinflammation impacts ODC mitochondrial Ca^{2+} buffering capacity, membrane potential, oxidative phosphorylation and production of metabolites by the tricarboxylic acid cycle (Martínez-Reyes & Chandel, 2020). Notably, the relative weight of these mitochondrial functions in relation to ODC and myelin homeostasis remain unclear. ODCs are described as glycolytic cells (Fünfschilling et al., 2012) and their mitochondria possess a relatively low surface area suggesting reduced ATP production compared to other CNS cell types (Rinholm et al., 2016; Rone et al., 2016). However, research on energetic dynamics in mature ODCs is a field in its infancy (Rosko et al., 2019). The different shape and density of mitochondria in processes and cytoplasmic myelin also suggests distinct organelle functions depending on the subcellular areas (N. Meyer & Rinholm, 2021). Ca^{2+} homeostasis in ODC mitochondria seems however an essential feature, as indicated by the generation of calcium waves (P. B. Simpson & Russell, 1996) and calcium transients during myelin remodeling (Battefeld et al., 2019).

Finally, given the reported differences between EAE-affected mice and MS patients in expression of ROS/RNS producing enzymes and in mechanisms amplifying oxidation (e.g., iron storages) (Schuh et al., 2014), the translational value of our animal-based work must be interpreted with caution.

To summarize, our study in ODC$^{mitoGFP-Tomato}$ mice provides the first in vivo description of the progressive pathological changes in ODC mitochondria upon induction of anti-myelin immunity. Our data indicate that ODC mitochondrial oxidation is a preclinical marker of autoimmune CNS inflammation and suggest that this early impairment might play a role in the subsequent evolution of ODC dysfunction.

CONFLICT OF INTEREST

The authors declare no conflicts of interest.

DATA AVAILABILITY STATEMENT

The data that support the findings of this study are available from the corresponding author upon reasonable request.

ORCID

Giuseppe Locatelli https://orcid.org/0000-0002-2179-4407

REFERENCES

Al-Kafaji, G., Bakheit, H. F., Al Ali, F., Fattah, M., Alhajeri, S., Alharbi, M. A., Daif, A., Alsabbagh, M. M., Alwehaidah, M. S., & Bakhiet, M. (2022). Next-generation sequencing of the whole mitochondrial genome identifies functionally deleterious mutations in patients with multiple sclerosis. *PLoS One*, *17*(2), e0263606. https://doi.org/10.1371/journal.pone.0263606

Barnett, M. H., & Prineas, J. W. (2004). Relapsing and remitting multiple sclerosis: Pathology of the newly forming lesion. *Annals of Neurology*, *55*(4), 458–468. https://doi.org/10.1002/ana.20016

Battefeld, A., Popovic, M. A., de Vries, S. I., & Kole, M. H. P. (2019). High-frequency microdomain ca(2+) transients and waves during early myelin internode remodeling. *Cell Reports*, *26*(1), 182–191. https://doi.org/10.1016/j.celrep.2018.12.039

Béchade, C., Colasse, S., Diana, M. A., Rouault, M., & Bessis, A. (2014). NOS2 expression is restricted to neurons in the healthy brain but is triggered in microglia upon inflammation. *Glia*, *62*(6), 956–963. https://doi.org/10.1002/glia.22652

Bedard, K., & Krause, K. H. (2007). The NOX family of ROS-generating NADPH oxidases: Physiology and pathophysiology. *Physiological Reviews*, *87*(1), 245–313. https://doi.org/10.1152/physrev.00044.2005

Billiau, A., & Matthys, P. (2001). Modes of action of Freund's adjuvants in experimental models of autoimmune diseases. *Journal of Leukocyte Biology*, *70*(6), 849–860.

Bolaños, J. P., Almeida, A., Stewart, V., Peuchen, S., Land, J. M., Clark, J. B., & Heales, S. J. (1997). Nitric oxide-mediated mitochondrial damage in the brain: Mechanisms and implications for neurodegenerative diseases. *Journal of Neurochemistry*, *68*(6), 2227–2240. https://doi.org/10.1046/j.1471-4159.1997.68062227.x

Breckwoldt, M. O., Pfister, F. M. J., Bradley, P. M., Marinković, P., Williams, P. R., Brill, M. S., Plomer, B., Schmalz, A., St Clair, D. K., Naumann, R., Griesbeck, O., Schwarzländer, M., Godinho, L., Bareyre, F. M., Dick, T. P., Kerschensteiner, M., & Misgeld, T. (2014). Multiparametric optical analysis of mitochondrial redox signals during neuronal physiology and pathology in vivo. *Nature Medicine*, *20*(5), 555–560. https://doi.org/10.1038/nm.3520

Chamberlain, K. A., Chapey, K. S., Nanescu, S. E., & Huang, J. K. (2017). Creatine enhances mitochondrial-mediated oligodendrocyte survival after demyelinating injury. *The Journal of Neuroscience*, *37*(6), 1479–1492. https://doi.org/10.1523/jneurosci.1941-16.2016

De Caterina, R., Libby, P., Peng, H. B., Thannickal, V. J., Rajavashisth, T. B., Gimbrone, M. A., Jr., Shin, W. S., & Liao, J. K. (1995). Nitric oxide decreases cytokine-induced endothelial activation. Nitric oxide selectively reduces endothelial expression of adhesion molecules and proinflammatory cytokines. *The Journal of Clinical Investigation*, *96*(1), 60–68. https://doi.org/10.1172/JCI118074

Frühbeis, C., Fröhlich, D., Kuo, W. P., Amphornrat, J., Thilemann, S., Saab, A. S., Kirchhoff, F., Möbius, W., Goebbels, S., Nave, K.-A., Schneider, A., Simons, M., Klugmann, M., Trotter, J., & Krämer-Albers, E.-M. (2013). Neurotransmitter-triggered transfer of exosomes mediates oligodendrocyte-neuron communication. *PLoS Biology*, *11*(7), e1001604. https://doi.org/10.1371/journal.pbio.1001604

Fujikawa, Y., Roma, L. P., Sobotta, M. C., Rose, A. J., Diaz, M. B., Locatelli, G., Breckwoldt, M. O., Misgeld, T., Kerschensteiner, M., Herzig, S., Müller-Decker, K., & Dick, T. P. (2016). Mouse redox histology using genetically encoded probes. *Science Signaling*, *9*(419), rs1. https://doi.org/10.1126/scisignal.aad3895

Fünfschilling, U., Supplie, L. M., Mahad, D., Boretius, S., Saab, A. S., Edgar, J., Brinkmann, B. G., Kassmann, C. M., Tzvetanova, I. D., Möbius, W., Diaz, F., Meijer, D., Suter, U., Hamprecht, B., Sereda, M. W., Moraes, C. T., Frahm, J., Goebbels, S., & Nave, K.-A. (2012). Glycolytic oligodendrocytes maintain myelin and long-term axonal integrity. *Nature*, *485*(7399), 517–521. https://doi.org/10.1038/nature11007

Garcia, G. C., Bartol, T. M., Phan, S., Bushong, E. A., Perkins, G., Sejnowski, T. J., Ellisman, M. H., & Skupin, A. (2019). Mitochondrial morphology provides a mechanism for energy buffering at synapses. *Scientific Reports*, *9*(1), 18306. https://doi.org/10.1038/s41598-019-54159-1

Gutscher, M., Sobotta, M. C., Wabnitz, G. H., Ballikaya, S., Meyer, A. J., Samstag, Y., & Dick, T. P. (2009). Proximity-based protein thiol oxidation by H2O2-scavenging peroxidases. *The Journal of Biological Chemistry*, *284*(46), 31532–31540. https://doi.org/10.1074/jbc.M109.059246

Haghayegh Jahromi, N., Tardent, H., Enzmann, G., Deutsch, U., Kawakami, N., Bittner, S., Vestweber, D., Zipp, F., Stein, J. V., & Engelhardt, B. (2017). A novel cervical spinal cord window preparation allows for two-photon imaging of T-cell interactions with the cervical spinal cord microvasculature during experimental autoimmune encephalomyelitis. *Frontiers in Immunology*, *8*, 406. https://doi.org/10.3389/fimmu.2017.00406

Haider, L., Fischer, M. T., Frischer, J. M., Bauer, J., Höftberger, R., Botond, G., Esterbauer, H., Binder, C. J., Witztum, J. L., & Lassmann, H. (2011). Oxidative damage in multiple sclerosis lesions. *Brain*, *134*(7), 1914–1924. https://doi.org/10.1093/brain/awr128

Hasseldam, H., Rasmussen, R. S., & Johansen, F. F. (2016). Oxidative damage and chemokine production dominate days before immune cell infiltration and EAE disease debut. *Journal of Neuroinflammation*, *13*(1), 246. https://doi.org/10.1186/s12974-016-0707-3

Higgins, G. C., Beart, P. M., Shin, Y. S., Chen, M. J., Cheung, N. S., & Nagley, P. (2010). Oxidative stress: Emerging mitochondrial and cellular themes and variations in neuronal injury. *Journal of Alzheimer's Disease*, *20*(2), S453–S473. https://doi.org/10.3233/jad-2010-100321

Hofstetter, H. H., Shive, C. L., & Forsthuber, T. G. (2002). Pertussis toxin modulates the immune response to neuroantigens injected in incomplete Freund's adjuvant: Induction of Th1 cells and experimental autoimmune encephalomyelitis in the presence of high frequencies of Th2 cells. *Journal of Immunology*, *169*(1), 117–125. https://doi.org/10.4049/jimmunol.169.1.117

Hoppins, S., Lackner, L., & Nunnari, J. (2007). The machines that divide and fuse mitochondria. *Annual Review of Biochemistry*, *76*, 751–780. https://doi.org/10.1146/annurev.biochem.76.071905.090048

Huynh, J. L., Garg, P., Thin, T. H., Yoo, S., Dutta, R., Trapp, B. D., Haroutunian, V., Zhu, J., Donovan, M. J., Sharp, A. J., & Casaccia, P. (2014). Epigenome-wide differences in pathology-free regions of multiple sclerosis-affected brains. *Nature Neuroscience*, *17*(1), 121–130. https://doi.org/10.1038/nn.3588

Ibrahim, W., Lee, U. S., Yen, H. C., St Clair, D. K., & Chow, C. K. (2000). Antioxidant and oxidative status in tissues of manganese superoxide dismutase transgenic mice. *Free Radical Biology & Medicine*, *28*(3), 397–402. https://doi.org/10.1016/s0891-5849(99)00253-1

Ivan, D. C., Walthert, S., Berve, K., Steudler, J., & Locatelli, G. (2021). Dwellers and trespassers: Mononuclear phagocytes at the borders of the central nervous system. *Frontiers in immunology*, *11*, 609921. https://doi.org/10.3389/fimmu.2020.609921

Jordão, M. J. C., Sankowski, R., Brendecke, S. M., Sagar, Locatelli, G., Tai, Y. H., Tay, T. L., Schramm, E., Armbruster, S., Hagemeyer, N., Groß, O., Mai, D., Çiçek, Ö., Falk, T., Kerschensteiner, M., Grün, D., & Prinz, M. (2019). Single-cell profiling identifies myeloid cell subsets with distinct fates during neuroinflammation. *Science*, *363*(6425), eaat7554. https://doi.org/10.1126/science.aat7554

Knott, A. B., Perkins, G., Schwarzenbacher, R., & Bossy-Wetzel, E. (2008). Mitochondrial fragmentation in neurodegeneration. *Nature Reviews Neuroscience*, 9(7), 505–518. https://doi.org/10.1038/nrn2417

Konradi, C., Sillivan, S. E., & Clay, H. B. (2012). Mitochondria, oligodendrocytes and inflammation in bipolar disorder: Evidence from transcriptome studies points to intriguing parallels with multiple sclerosis. *Neurobiology of Disease*, 45(1), 37–47. https://doi.org/10.1016/j.nbd.2011.01.025

Lacza, Z., Kozlov, A. V., Pankotai, E., Csordás, A., Wolf, G., Redl, H., Kollai, M., Szabó, C., Busija, D. W., & Horn, T. F. (2006). Mitochondria produce reactive nitrogen species via an arginine-independent pathway. *Free Radical Research*, 40(4), 369–378. https://doi.org/10.1080/10715760500539139

Lan, M., Tang, X., Zhang, J., & Yao, Z. (2018). Insights in pathogenesis of multiple sclerosis: Nitric oxide may induce mitochondrial dysfunction of oligodendrocytes. *Reviews in the Neurosciences*, 29(1), 39–53. https://doi.org/10.1515/revneuro-2017-0033

Lassmann, H., & van Horssen, J. (2016). Oxidative stress and its impact on neurons and glia in multiple sclerosis lesions. *Biochimica et Biophysica Acta (BBA) - Molecular Basis of Disease*, 1862(3), 506–510. https://doi.org/10.1016/j.bbadis.2015.09.018

Ledo, A., Fernandes, E., Salvador, A., Laranjinha, J., & Barbosa, R. M. (2022). In vivo hydrogen peroxide diffusivity in brain tissue supports volume signaling activity. *Redox Biology*, 50, 102250. https://doi.org/10.1016/j.redox.2022.102250

Lee, C., Nam, J. S., Lee, C. G., Park, M., Yoo, C.-M., Rhee, H.-W., Seo, J. K., & Kwon, T.-H. (2021). Analysing the mechanism of mitochondrial oxidation-induced cell death using a multifunctional iridium(III) photosensitiser. *Nature Communications*, 12(1), 26. https://doi.org/10.1038/s41467-020-20210-3

Lee, Y., Morrison, B. M., Li, Y., Lengacher, S., Farah, M. H., Hoffman, P. N., Liu, Y., Tsingalia, A., Jin, L., Zhang, P.-W., Pellerin, L., Magistretti, P. J., & Rothstein, J. D. (2012). Oligodendroglia metabolically support axons and contribute to neurodegeneration. *Nature*, 487(7408), 443–448. https://doi.org/10.1038/nature11314

Locatelli, G., Theodorou, D., Kendirli, A., Jordão, M. J. C., Staszewski, O., Phulphagar, K., Cantuti-Castelvetri, L., Dagkalis, A., Bessis, A., Simons, M., Meissner, F., Prinz, M., & Kerschensteiner, M. (2018). Mononuclear phagocytes locally specify and adapt their phenotype in a multiple sclerosis model. *Nature Neuroscience*, 21(9), 1196–1208. https://doi.org/10.1038/s41593-018-0212-3

Locatelli, G., Wörtge, S., Buch, T., Ingold, B., Frommer, F., Sobottka, B., Krüger, M., Karram, K., Bühlmann, C., Bechmann, I., Heppner, F. L., Waisman, A., & Becher, B. (2012). Primary oligodendrocyte death does not elicit anti-CNS immunity. *Nature Neuroscience*, 15(4), 543–550. https://doi.org/10.1038/nn.3062

López-Juárez, A., Titus, H. E., Silbak, S. H., Pressler, J. W., Rizvi, T. A., Bogard, M., Bennett, M. R., Ciraolo, G., Williams, M. T., Vorhees, C. V., & Ratner, N. (2017). Oligodendrocyte Nf1 controls aberrant notch activation and regulates myelin structure and behavior. *Cell Reports*, 19(3), 545–557. https://doi.org/10.1016/j.celrep.2017.03.073

Lucchinetti, C., Brück, W., Parisi, J., Scheithauer, B., Rodriguez, M., & Lassmann, H. (1999). A quantitative analysis of oligodendrocytes in multiple sclerosis lesions. A study of 113 cases. *Brain*, 122(12), 2279–2295. https://doi.org/10.1093/brain/122.12.2279

Madisen, L., Zwingman, T. A., Sunkin, S. M., Oh, S. W., Zariwala, H. A., Gu, H., Ng, L. L., Palmiter, R. D., Hawrylycz, M. J., Jones, A. R., Lein, E. S., & Zeng, H. (2010). A robust and high-throughput Cre reporting and characterization system for the whole mouse brain. *Nature Neuroscience*, 13(1), 133–140. https://doi.org/10.1038/nn.2467

Mahad, D., Ziabreva, I., Lassmann, H., & Turnbull, D. (2008). Mitochondrial defects in acute multiple sclerosis lesions. *Brain*, 131(7), 1722–1735. https://doi.org/10.1093/brain/awn105

Mahad, D. H., Trapp, B. D., & Lassmann, H. (2015). Pathological mechanisms in progressive multiple sclerosis. *Lancet Neurology*, 14(2), 183–193. https://doi.org/10.1016/s1474-4422(14)70256-x

Martínez-Reyes, I., & Chandel, N. S. (2020). Mitochondrial TCA cycle metabolites control physiology and disease. *Nature Communications*, 11(1), 102. https://doi.org/10.1038/s41467-019-13668-3

McIver, S. R., Muccigrosso, M., Gonzales, E. R., Lee, J. M., Roberts, M. S., Sands, M. S., & Goldberg, M. P. (2010). Oligodendrocyte degeneration and recovery after focal cerebral ischemia. *Neuroscience*, 169(3), 1364–1375. https://doi.org/10.1016/j.neuroscience.2010.04.070

McTigue, D. M., & Tripathi, R. B. (2008). The life, death, and replacement of oligodendrocytes in the adult CNS. *Journal of Neurochemistry*, 107(1), 1–19. https://doi.org/10.1111/j.1471-4159.2008.05570.x

Mendiola, A. S., Ryu, J. K., Bardehle, S., Meyer-Franke, A., Ang, K. K.-H., Wilson, C., Baeten, K. M., Hanspers, K., Merlini, M., Thomas, S., Petersen, M. A., Williams, A., Thomas, R., Rafalski, V. A., Meza-Acevedo, R., Tognatta, R., Yan, Z., Pfaff, S. J., Machado, M. R., … Akassoglou, K. (2020). Transcriptional profiling and therapeutic targeting of oxidative stress in neuroinflammation. *Nature Immunology*, 21(5), 513–524. https://doi.org/10.1038/s41590-020-0654-0

Metz, I., Weigand, S. D., Popescu, B. F., Frischer, J. M., Parisi, J. E., Guo, Y., Lassmann, H., Brück, W., & Lucchinetti, C. F. (2014). Pathologic heterogeneity persists in early active multiple sclerosis lesions. *Annals of Neurology*, 75(5), 728–738. https://doi.org/10.1002/ana.24163

Meyer, A. J., & Dick, T. P. (2010). Fluorescent protein-based redox probes. *Antioxidants & Redox Signaling*, 13(5), 621–650. https://doi.org/10.1089/ars.2009.2948

Meyer, N., & Rinholm, J. E. (2021). Mitochondria in myelinating oligodendrocytes: Slow and out of breath? *Metabolites*, 11(6), 359. https://doi.org/10.3390/metabo11060359

Minchenberg, S. B., & Massa, P. T. (2019). The control of oligodendrocyte bioenergetics by interferon-gamma (IFN-γ) and Src homology region 2 domain-containing phosphatase-1 (SHP-1). *Journal of Neuroimmunology*, 331, 46–57. https://doi.org/10.1016/j.jneuroim.2017.10.015

Mishra, M. K., & Yong, V. W. (2016). Myeloid cells — Targets of medication in multiple sclerosis. *Nature Reviews Neurology*, 12(9), 539–551. https://doi.org/10.1038/nrneurol.2016.110

Moore, S., Meschkat, M., Ruhwedel, T., Trevisiol, A., Tzvetanova, I. D., Battefeld, A., Kusch, K., Kole, M. H. P., Strenzke, N., Möbius, W., de Hoz, L., & Nave, K.-A. (2020). A role of oligodendrocytes in information processing. *Nature Communications*, 11(1), 5497. https://doi.org/10.1038/s41467-020-19152-7

Mronga, T., Stahnke, T., Goldbaum, O., & Richter-Landsberg, C. (2004). Mitochondrial pathway is involved in hydrogen-peroxide-induced apoptotic cell death of oligodendrocytes. *Glia*, 46(4), 446–455. https://doi.org/10.1002/glia.20022

Müller, A., Schneider, J. F., Degrossoli, A., Lupilova, N., Dick, T. P., & Leichert, L. I. (2017). Systematic in vitro assessment of responses of roGFP2-based probes to physiologically relevant oxidant species. *Free Radical Biology & Medicine*, 106, 329–338. https://doi.org/10.1016/j.freeradbiomed.2017.02.044

Murphy, M. P. (2009). How mitochondria produce reactive oxygen species. *The Biochemical Journal*, 417(1), 1–13. https://doi.org/10.1042/bj20081386

Murray, P. J., & Wynn, T. A. (2011). Protective and pathogenic functions of macrophage subsets. *Nature Reviews Immunology*, 11(11), 723–737. https://doi.org/10.1038/nri3073

Nellessen, A., Nyamoya, S., Zendedel, A., Slowik, A., Wruck, C., Beyer, C., Fragoulis, A., & Clarner, T. (2020). Nrf2 deficiency increases oligodendrocyte loss, demyelination, neuroinflammation and axonal damage in an MS animal model. *Metabolic Brain Disease*, 35(2), 353–362. https://doi.org/10.1007/s11011-019-00488-z

Niedbala, W., Alves-Filho Jose, C., Fukada Sandra, Y., Vieira Silvio, M., Mitani, A., Sonego, F., Mirchandani, A., Nascimento Daniele, C., Cunha Fernando, Q., & Liew Foo, Y. (2011). Regulation of type 17 helper T-

cell function by nitric oxide during inflammation. *Proceedings of the National Academy of Sciences*, *108*(22), 9220–9225. https://doi.org/10.1073/pnas.1100667108

Nikić, I., Merkler, D., Sorbara, C., Brinkoetter, M., Kreutzfeldt, M., Bareyre, F. M., Brück, W., Bishop, D., Misgeld, T., & Kerschensteiner, M. (2011). A reversible form of axon damage in experimental autoimmune encephalomyelitis and multiple sclerosis. *Nature Medicine*, *17*(4), 495–499. https://doi.org/10.1038/nm.2324

Poursadegh Zonouzi, A., Ghorbian, S., Abkar, M., Poursadegh Zonouzi, A. A., & Azadi, A. (2014). Mitochondrial complex I gene variations; as a potential genetic risk factor in pathogenesis of multiple sclerosis. *Journal of the Neurological Sciences*, *345*(1–2), 220–223. https://doi.org/10.1016/j.jns.2014.07.051

Qi, X., Lewin, A. S., Sun, L., Hauswirth, W. W., & Guy, J. (2006). Mitochondrial protein nitration primes neurodegeneration in experimental autoimmune encephalomyelitis. *The Journal of Biological Chemistry*, *281*(42), 31950–31962. https://doi.org/10.1074/jbc.M603717200

Rath, M., Müller, I., Kropf, P., Closs, E. I., & Munder, M. (2014). Metabolism via arginase or nitric oxide synthase: Two competing arginine pathways in macrophages. *Frontiers in Immunology*, *5*, 1–10. https://doi.org/10.3389/fimmu.2014.00532

Rinholm, J. E., Vervaeke, K., Tadross, M. R., Tkachuk, A. N., Kopek, B. G., Brown, T. A., Bergersen, L. H., & Clayton, D. A. (2016). Movement and structure of mitochondria in oligodendrocytes and their myelin sheaths. *Glia*, *64*(5), 810–825. https://doi.org/10.1002/glia.22965

Romanelli, E., Merkler, D., Mezydlo, A., Weil, M.-T., Weber, M. S., Nikić, I., Potz, S., Meinl, E., Matznick, F. E. H., Kreutzfeldt, M., Ghanem, A., Conzelmann, K.-K., Metz, I., Brück, W., Routh, M., Simons, M., Bishop, D., Misgeld, T., & Kerschensteiner, M. (2016). Myelinosome formation represents an early stage of oligodendrocyte damage in multiple sclerosis and its animal model. *Nature Communications*, *7*(1), 13275. https://doi.org/10.1038/ncomms13275

Romanelli, E., Sorbara, C. D., Nikić, I., Dagkalis, A., Misgeld, T., & Kerschensteiner, M. (2013). Cellular, subcellular and functional in vivo labeling of the spinal cord using vital dyes. *Nature Protocols*, *8*(3), 481–490. https://doi.org/10.1038/nprot.2013.022

Rone, M. B., Cui, Q. L., Fang, J., Wang, L. C., Zhang, J., Khan, D., Bedard, M., Almazan, G., Ludwin, S. K., Jones, R., Kennedy, T. E., & Antel, J. P. (2016). Oligodendrogliopathy in multiple sclerosis: Low glycolytic metabolic rate promotes oligodendrocyte survival. *The Journal of Neuroscience*, *36*(17), 4698–4707. https://doi.org/10.1523/jneurosci.4077-15.2016

Rose, J., Brian, C., Woods, J., Pappa, A., Panayiotidis, M. I., Powers, R., & Franco, R. (2017). Mitochondrial dysfunction in glial cells: Implications for neuronal homeostasis and survival. *Toxicology*, *391*, 109–115. https://doi.org/10.1016/j.tox.2017.06.011

Rosko, L., Smith, V. N., Yamazaki, R., & Huang, J. K. (2019). Oligodendrocyte bioenergetics in health and disease. *The Neuroscientist*, *25*(4), 334–343. https://doi.org/10.1177/1073858418793077

Roth, A. D., & Núñez, M. T. (2016). Oligodendrocytes: Functioning in a delicate balance between high metabolic requirements and oxidative damage. *Advances in Experimental Medicine and Biology*, *949*, 167–181. https://doi.org/10.1007/978-3-319-40764-7_8

Saederup, N., Cardona, A. E., Croft, K., Mizutani, M., Cotleur, A. C., Tsou, C. L., Ransohoff, R. M., & Charo, I. F. (2010). Selective chemokine receptor usage by central nervous system myeloid cells in CCR2-red fluorescent protein knock-in mice. *PLoS One*, *5*(10), e13693. https://doi.org/10.1371/journal.pone.0013693

Sanchez-Padilla, J., Guzman, J. N., Ilijic, E., Kondapalli, J., Galtieri, D. J., Yang, B., Schieber, S., Oertel, W., Wokosin, D., Schumacker, P. T., & Surmeier, D. J. (2014). Mitochondrial oxidant stress in locus coeruleus is regulated by activity and nitric oxide synthase. *Nature Neuroscience*, *17*(6), 832–840. https://doi.org/10.1038/nn.3717

Sanmarco, L. M., Polonio, C. M., Wheeler, M. A., & Quintana, F. J. (2021). Functional immune cell-astrocyte interactions. *The Journal of Experimental Medicine*, *218*(9), 1–11. https://doi.org/10.1084/jem.20202715

Santos, R. M., Lourenço, C. F., Pomerleau, F., Huettl, P., Gerhardt, G. A., Laranjinha, J., & Barbosa, R. M. (2010). Brain nitric oxide inactivation is governed by the vasculature. *Antioxidants & Redox Signaling*, *14*(6), 1011–1021. https://doi.org/10.1089/ars.2010.3297

Scheld, M., Fragoulis, A., Nyamoya, S., Zendedel, A., Denecke, B., Krauspe, B., Teske, N., Kipp, M., Beyer, C., & Clarner, T. (2019). Mitochondrial impairment in oligodendroglial cells induces cytokine expression and signaling. *Journal of Molecular Neuroscience*, *67*(2), 265–275. https://doi.org/10.1007/s12031-018-1236-6

Schindelin, J., Arganda-Carreras, I., Frise, E., Kaynig, V., Longair, M., Pietzsch, T., Preibisch, S., Rueden, C., Saalfeld, S., Schmid, B., Tinevez, J.-Y., White, D. J., Hartenstein, V., Eliceiri, K., Tomancak, P., & Cardona, A. (2012). Fiji: An open-source platform for biological-image analysis. *Nature Methods*, *9*(7), 676–682. https://doi.org/10.1038/nmeth.2019

Schuh, C., Wimmer, I., Hametner, S., Haider, L., Van Dam, A.-M., Liblau, R. S., Smith, K. J., Probert, L., Binder, C. J., Bauer, J., Bradl, M., Mahad, D., & Lassmann, H. (2014). Oxidative tissue injury in multiple sclerosis is only partly reflected in experimental disease models. *Acta Neuropathologica*, *128*(2), 247–266. https://doi.org/10.1007/s00401-014-1263-5

Simpson, D. S. A., & Oliver, P. L. (2020). ROS generation in microglia: Understanding oxidative stress and inflammation in neurodegenerative disease. *Antioxidants (Basel)*, *9*(8), 1–27. https://doi.org/10.3390/antiox9080743

Simpson, P. B., & Russell, J. T. (1996). Mitochondria support inositol 1,4,5-trisphosphate-mediated $Ca2+$ waves in cultured oligodendrocytes. *Journal of Biological Chemistry*, *271*(52), 33493–33501. https://doi.org/10.1074/jbc.271.52.33493

Smith, K. J. (2011). Newly lesioned tissue in multiple sclerosis—A role for oxidative damage? *Brain*, *134*(7), 1877–1881. https://doi.org/10.1093/brain/awr144

Tang, X., Lan, M., Zhang, M., & Yao, Z. (2017). Effect of nitric oxide to axonal degeneration in multiple sclerosis via downregulating monocarboxylate transporter 1 in oligodendrocytes. *Nitric Oxide*, *67*, 75–80. https://doi.org/10.1016/j.niox.2017.04.004

Tengan, C. H., & Moraes, C. T. (2017). NO control of mitochondrial function in normal and transformed cells. *Biochimica et Biophysica Acta - Bioenergetics*, *1858*(8), 573–581. https://doi.org/10.1016/j.bbabio.2017.02.009

Tietz, S. M., Zwahlen, M., Haghayegh Jahromi, N., Baden, P., Lazarevic, I., Enzmann, G., & Engelhardt, B. (2016). Refined clinical scoring in comparative EAE studies does not enhance the chance to observe statistically significant differences. *European Journal of Immunology*, *46*(10), 2481–2483. https://doi.org/10.1002/eji.201546272

Todorich, B., Pasquini, J. M., Garcia, C. I., Paez, P. M., & Connor, J. R. (2009). Oligodendrocytes and myelination: The role of iron. *Glia*, *57*(5), 467–478. https://doi.org/10.1002/glia.20784

Tondera, D., Grandemange, S., Jourdain, A., Karbowski, M., Mattenberger, Y., Herzig, S., Da Cruz, S., Clerc, P., Raschke, I., Merkwirth, C., Ehses, S., Krause, F., Chan, D. C., Alexander, C., Bauer, C., Youle, R., Langer, T., & Martinou, J. C. (2009). SLP-2 is required for stress-induced mitochondrial hyperfusion. *The EMBO Journal*, *28*(11), 1589–1600. https://doi.org/10.1038/emboj.2009.89

Trachootham, D., Lu, W., Ogasawara, M. A., Nilsa, R. D., & Huang, P. (2008). Redox regulation of cell survival. *Antioxidants & Redox Signaling*, *10*(8), 1343–1374. https://doi.org/10.1089/ars.2007.1957

Twig, G., Elorza, A., Molina, A. J., Mohamed, H., Wikstrom, J. D., Walzer, G., Stiles, L., Haigh, S. E., Katz, S., Las, G., Alroy, J., Wu, M., Py, B. F., Yuan, J., Deeney, J. T., Corkey, B. E., & Shirihai, O. S. (2008). Fission and selective fusion govern mitochondrial segregation and

elimination by autophagy. *The EMBO Journal, 27*(2), 433–446. https://doi.org/10.1038/sj.emboj.7601963

Vladymyrov, M., Abe, J., Moalli, F., Stein, J. V., & Ariga, A. (2016). Real-time tissue offset correction system for intravital multiphoton microscopy. *Journal of Immunological Methods, 438*, 35–41. https://doi.org/10.1016/j.jim.2016.08.004

Vladymyrov, M., Haghayegh Jahromi, N., Kaba, E., Engelhardt, B., & Ariga, A. (2020). VivoFollow 2: Distortion-free multiphoton Intravital imaging. *Frontiers in Physics, 7*, 12. https://doi.org/10.3389/fphy.2019.00222

Witte, M. E., Mahad, D. J., Lassmann, H., & van Horssen, J. (2014). Mitochondrial dysfunction contributes to neurodegeneration in multiple sclerosis. *Trends in Molecular Medicine, 20*(3), 179–187. https://doi.org/10.1016/j.molmed.2013.11.007

Wolswijk, G. (2000). Oligodendrocyte survival, loss and birth in lesions of chronic-stage multiple sclerosis. *Brain, 123*(1), 105–115. https://doi.org/10.1093/brain/123.1.105

Wu, S., Zhou, F., Zhang, Z., & Xing, D. (2011). Mitochondrial oxidative stress causes mitochondrial fragmentation via differential modulation of mitochondrial fission-fusion proteins. *The FEBS Journal, 278*(6), 941–954. https://doi.org/10.1111/j.1742-4658.2011.08010.x

Yamasaki, R., Lu, H., Butovsky, O., Ohno, N., Rietsch, A. M., Cialic, R., Wu, P. M., Doykan, C. E., Lin, J., Cotleur, A. C., Kidd, G., Zorlu, M. M., Sun, N., Hu, W., Liu, L., Lee, J. C., Taylor, S. E., Uehlein, L., Dixon, D., ... Ransohoff, R. M. (2014). Differential roles of microglia and monocytes in the inflamed central nervous system. *The Journal of Experimental Medicine, 211*(8), 1533–1549. https://doi.org/10.1084/jem.20132477

Zeis, T., & Schaeren-Wiemers, N. (2008). Lame ducks or fierce creatures? The role of oligodendrocytes in multiple sclerosis. *Journal of Molecular Neuroscience, 35*(1), 91–100. https://doi.org/10.1007/s12031-008-9042-1

SUPPORTING INFORMATION

Additional supporting information can be found online in the Supporting Information section at the end of this article.